

Segmentation of Pelvic Arteries to Image Guided Radiotherapy



By Asger Hammarberg Andresen
Biomedical Engineering and Informatics
10. Semester at Aalborg University

Title:

Segmentation of pelvic arteries to image guided radiotherapy

Project Period:

4rd Semester - Master, Spring 2011

Project Group:

Group 1086h

Participants:

Asger Hammarberg Andresen

Supervisors:

Lasse Riis Østergaard

Copies: 3

Pages: 72

Appendices: 0

Finished: August 31st 2011

Image guided radiotherapy is selective in the targeting of cancerous tissue. An automatic detailed delineation of the clinical target volume may decrease the treatment planning and inter-variability among clinicians. The aim of this work is to develop a vessel segmentation method to indirectly detect lymph nodes with poor visual appearance in medical images. The method is designed with three stages. First stage uses a region growing method to extract an initial vessel tree volume. Stage two use elliptic vessel cross section features to define tube like vessel segments originally developed for image-guided peripheral bronchoscopy. Stage three connects the vessel tree volume from stage one and the vessel segments from stage two. The method is semiautomatic and only requires one manual selected seed voxel.

Fourteen bolus tracked CTA data sets were used in the test. The initial segmentation method in stage one was able to automatically select a threshold and extract an initial vessel tree without over segmentation. In addition a bone filter successfully removed bone structure. The full segmentation method was able to extend the initial vessel tree with the defined vessel segments from stage two. However, the final extracted vessel volume was prone to over segmentation, which may be caused by selected computational delimitations in the method design. Several parameters in the method enable optimisation and since the quality of the CTA data varies, the potential of the method is not fully elaborated.

In conclusion the segmentation method shows beneficial results and may potentially improve the extraction of vessel volume to guide radiotherapy.

Preface

Asger Hammarberg Andresen has prepared this thesis at the Institute of Health Science and Technology, at Aalborg University. The report is the master thesis of Biomedical Engineering and Informatics, and was completed in the period from February the 1st to August the 31st 2011.

References in this report are stated according to the Harvard-method, where the author and year is cited as: [author,year]. Citations prior to a full stop only refers to the last sentence. However, if the citations follow directly after a full stop it refers to the paragraph or section.

The report is divided in five parts. The first part is named 'Background' and contains a pre analysis that leads to a problem statement. The second part follows an analysis based on the problem statement. In the third part named 'Method' is the method as a solution to the problem statement described. In the fourth part named 'Test' is the test of the applied method described. The fifth and last part contains the recapitulation of the report and includes a discussion on the test results, a conclusion on the work and suggestion to future work.

Acknowledgments

A thanks to Chief physicist Jesper Carl for providing CT data for this work.

This report was prepared by:

Asger Hammarberg Andresen

Contents

1	Introduction	8
I	Background	10
2	Treatments	11
3	Conventional Radiotherapy	13
3.1	Determine The Target Volumes	13
3.2	Image Guided Radiotherapy	15
3.3	The Challenge of Lymph Node Delineation	16
4	The Arteries as Surrogate	17
4.1	Lymph Nodes of Interest	17
4.2	Pelvic Arteries	18
5	Problem Statement	20
II	Analysis	22
6	Research in Vessel Segmentation	23
6.1	Image Features	23
6.2	Extraction Schemes	24
7	Data Analysis	26
7.1	The Data	26
7.2	Vessel Appearance	26
7.3	Artefacts	30
III	Method	31
8	Applied Segmentation Method	32
8.1	Method Introduction	32
8.2	Overview of the Segmentation Method	34
9	Stage 1: Initial Segmentation	35

10 Stage 2: Extended Segmentation	38
10.1 Detection of Vessel Cross Sections	38
10.2 Define Vessel Segments	42
10.3 Extended Vs. Original Method	45
11 Stage 3: Merge Segmentations	46
11.1 The Merging of Extracted Volumes	46
11.2 Implementation	48
IV Test	49
12 Test	50
12.1 The Initial Segmentation	50
12.1.1 Selection of Threshold	50
12.1.2 The Initial Vessel Tree	52
12.1.3 Bone Filtering	53
12.2 The Extended Segmentation	54
12.2.1 Extracted Segments	54
12.2.2 Performance of Segmentation	56
12.3 Segmentation Profiles	57
V Recapitulation	64
13 Discussion	65
13.1 Summary	65
13.2 Discussion	66
13.3 Conclusion	67
13.4 Future Work	68

Chapter 1

Introduction

Cancer has one of the highest mortalities in the world [WHO, 2011] and the incident of patients with diagnosed cancer shows an increasing tendency in all countries with reliable reporting. In Denmark the prevalence is 230,000 and the incident is 33,000 per year [Rørth and Hansen, 2009; Cancer.dk, 2011].

Pelvic cancer refers to cancer in the anatomical location of pelvic and contains two thirds of all classified cancers (with lower abdomen) [Lengelé and Scalliet, 2009]. Among the typical pelvic cancers are colon, rectal, prostate and gynaecologic cancers. In Denmark for example more than 2,600 was diagnosed with either gynaecologic or prostate cancer (in 2001), which is approximately eight percent of all diagnosed cancers. In general 27.9 percent of diagnosed cancers are pelvic cancer.[Clemmensen et al., 2006]

The cancer disease is defined as the presence of a malign tumor, which has a dysfunctional cellular production. The malign tumor consists of cells with mutated DNA, distinguished from a normal cluster of cells by shape and abnormal size.[Martini, 2006a]

The state of the malign tumor depends mainly on three characteristics: An accelerated cell population growth, an invasive cell growth and the cells ability to spread to surrounding tissues and distant regions.

The first tumor appearance is defined as the primary tumor and the secondary tumor is established when cancer cells are spreading to distant regions of the body, where the secondary tumor is located also called 'metastasis'.

Metastasis begins by a tumor break from the primary tumor, containing a large amount of cancer cells, which are spreading mainly through the lymphatic system or blood circulation. When metastasis enters the lymphatic system the cancer cells are accumulating in the lymphatic nodes and progress in stages along the nodes. If the metastasis enters the blood stream the cancer cells may circulate throughout the entire body. [Rørth and Hansen, 2009; Martini, 2006b]

Metastasis occurs in two thirds of every cancer patients and may reach every organ in the body. The cancer cells have an inactive or abnormal function and compete with normal cells in obtaining space and nutrients. In the end the cancer cells replace healthy cells in vital organs or cause important nutrients starvations in the body, which leads to organ failure and death.[Rørth and Hansen, 2009; Martini, 2006b]

The diagnosis of cancer is obtained by a review of the clinical history and noting symptoms. During the patient examination the clinician uses laboratory test to detect unusual test result numbers

that may relate to cancer. This can be by analysing urine, blood or other physical examinations. Imaging diagnostic tools e.g. CT and MRI images are important, especially in localizing the tumor and providing visual interpretation of the disease progression.[Rørth, 2007; Britannica, 2011; Institute, 2011]

One of the most important aspects in the clinical course is cancer staging, which help treatment planning, evaluation, prognosis and more. Several systems have been developed to determine the stage, and some are more applicable depending on the case. However, the most popular is the 'TNM' system, which is used widely in the clinic and stands for Primary Tumor (T), Regional Lymph Nodes (N) and Distant Metastasis (M). Each element contains different ratings corresponding to the severity of the cancer stage. [Souhami, 2008a; Institute, 2011]

The involvement of the lymph is probably the most important determinant of survival[Souhami, 2008a], and since patients with pelvic cancer often have lymph node metastasis[Dinniwell et al., 2009], it stresses the importance of avoiding cancer progression by treating malignly in the lymphatic system.

The purpose of the lymphatic system is to defend the body against internal threats such as infections and diseases. The system consists of lymph fluid, a network of lymph vessels originate periphery and end in connection with vein vessels, lymphoid tissue, lymphoid organs, lymphocytes, phagocytes and other cells. [Martini, 2006b]

A lymph node is a lymphatic organ ranging in diameter from 1 mm to 25 mm and has the main purposes of warning the body against threats and slowing down the progression of the threats. When cancer cells are detected the lymph nodes activates a defence mechanism within the node causing an excessive enlargement. [Martini, 2006b] A lymph node diameter greater than 1 cm(the short axis) or a biopsy determines if the node is pat logic [van de Bunt et al., 2006].

Since metastasis in the lymph nodes is common in patients with pelvic cancer [Dinniwell et al., 2009] and an important indicator of cancer prognosis, there can be a significant beneficial effect by treating cancer progression in the lymphatic system. Thereby, the motivation is to investigate how the treatment of pelvic cancer can be improved by reducing the cancer progression via the lymphatic nodes. This report describes an approach to improve the treatment of cancer by using image analysis.

Part I

Background

Chapter 2

Treatments

In this chapter the treatment options for cancer are presented to provide an overview. The treatment options are surgery, medicine and radiotherapy, or in a combination. Within each treatment there is a span of varieties to make specific treatment adjustment to the patient. Today, therapies including all three main treatments are increasingly becoming a standard approach in oncology centres [Rørth and Hansen, 2009]. Note that this chapter is mainly based on [Rørth and Hansen, 2009; Rørth, 2007]

Medical Treatment

Most of the medical treatments are targeted at achieving cytotoxic effects to limit the growth of the malign tumour or to obtain cell death. The medical treatment is performed with the administering of the pharmacy called 'Antineoplastics'. However some hormone sensitive cancers can be treated with hormones and a few patients can benefit from medicine with immunoregulatory effects.

The arsenal of antineoplastics has reached approximately 60 different types and antineoplastics appear in many complex combinations to treat the different kinds of cancers. This treatment is known as 'Chemotherapy' and covers administration of antineoplastics intravenously, intramuscularly or orally.

There is the systemic chemotherapy, where antineoplastics enters the blood stream and are distributed throughout the system. On the other hand the impact of regional chemotherapy is a limited area of the body. The aim of regional chemotherapy is to only affect the target region and thereby reducing side effects. However, the treatment option is based on the diagnosis and cancer state.

The antineoplastics are toxic for the cancer cells and the normal cells. The administration therefore requires detailed knowledge about molecular regulatory effects. Chemotherapy remains non selective and aims at obtaining a quantitative difference in cancer cell reduction between the cancer and normal cell group.

Since a sensitivity test of the cancer cell is not yet clinical available, the choice of antineoplastics is still based on 'trial and error' and the dosage is also determined empirically. The cytotoxic effect is proportional to dosage magnitude however, an increase in dosage also affects normal cells due to overlapping spectrum. Therefore the approach is to repeat the treatment and use combinations of antineoplastics to reduce the overlapping side effect.

The use of antineoplastics has experienced an increase the last couple of years, which is explained

by more effective treatments, reduced side effects, new antineoplastics and more.

Radiotherapy

The basics of radiotherapy are x-ray irradiation of cancer cells to minimize the cell growth and perform cell death. The radiotherapy can be used alone or in combinations with surgical and medical treatments. E. g. Chemotherapy or hormonal treatment may improve the outcome of radiotherapy.

Radiotherapy is applied either by external equipment or internal by e. g. implementation of radioactive needles. Ideally the radiotherapy is very selective to kill cancer cells, however in the clinics the radiotherapy cause tissue damage in the adjacent tissue and local areas.

Today new radiation equipment decreases the complication and the introduction of MRI and CT modalities have improved the planning of the therapy. The new tools help with a more precisely determination of a target area, which has a radical reduction in adjacent tissue damage and thereby reduces the side effects.

Surgery

In curative surgical therapy the goal is to remove the malign tumor by making a surgical intervention. At time of cancer diagnosis, more than half of the patients have tumors available for surgical intervention. In these cases the surgical goal is to remove the tumor as a whole. However, the removal of the tumor may not affect the metastasis if cells with potential to develop metastasis are already in circulation.

Surgical intervention in general plays an important role in terms of diagnosis, determination of the cancer state and sub-classification and is always necessary (Except in leukaemia).

In a report from the Royal College of Radiologists the curative effects (of the patients cured) are estimated to 49 % with surgery, 40% by radiotherapy and 11% by chemotherapy[Souhami, 2008b]. Since surgery is mostly effective in early stages to remove the primary tumor, the progression in the lymphatic system does not normally suggest a surgical intervention. The conventional chemotherapy remains non-selective and very complex, due to overlapping toxicity spectrum of cancer and normal cells.

The radiotherapy is one of the standard treatments of several cancer diseases in combination with surgery or/and chemotherapy. However, radiotherapy does have a preferable advantage due to the preferential cytotoxic for cancerous cells relative to normal cells. [David Jaffray and Gospodarowicz, 2008] In addition the treatment is very selective when treating lymph nodes and has a relative few side effects. Today the radiotherapy is already important in the treatment of many pelvic malignancies [Taylor et al., 2007], and at some point 40% of all patients requires radiotherapy[Souhami, 2008b]. Thus in the following chapter the focus is radiotherapy.

Chapter 3

Conventional Radiotherapy

In this chapter the conventional radiotherapy is described. The first section contains an introduction to how the clinician determines the target volumes. In the next section the side effects and medical images used in radiotherapy are briefly presented. The following section contains a presentation of Image Guided Radiotherapy (IGRT) and especially Intensity Modulated Radiotherapy (IMRT). In the last section the challenge of lymph node delineation is described.

3.1 Determine The Target Volumes

Ideally the aim of radiotherapy is to irradiate the malign tumor as a whole and at the same time spare the adjacent normal tissue. To approach this the treatment follows a planning phase where the clinicians use medical images to characterise and detect target volumes that should undergo irradiation.

The targeting of cancer volumes is highly complex due to the invasive entanglement into healthy tissue areas. Some target volumes are intertwined with critical organs while other target volumes are nicely isolated. The slightest cancer residuals impose a high risk of cancer recurrence due to the aggressive nature of cancer cells. Therefore a confident eradication is needed to ensure full coverage of the cancer tissue. Thus treatment must compromise the sparing of healthy tissue and thereby cause side effects.

The definition of target volumes follows the standard published by "The International Commission of Radiological Units", which also uses the principles of explicitly define geometric margins to locate the radiation dose distribution. [David Jaffray and Gospodarowicz, 2008; Cefaro et al., 2008] This accommodates the technical challenge in planning the radiation dose in areas of co localised healthy tissue and cancer tissue.

The standard volumes are illustrated in figure 3.1 and are known as Gross Tumor Volume (GTV) including the macroscopic or known tumor, Clinical Target Volume (CTV), including the volume with suspected microscopic spread and Planning Target Volume (PTV) which covers the necessary marginal volume that compensates for setup variations, organ and patient motion. In addition there is an Organ At Risk (OAR) volume to constrain the dose if there is certain critical organ that must be spared e. g. rectum and bladder. To avoid the OAR the clinicians also use the Planning Risk Volume (PRV).

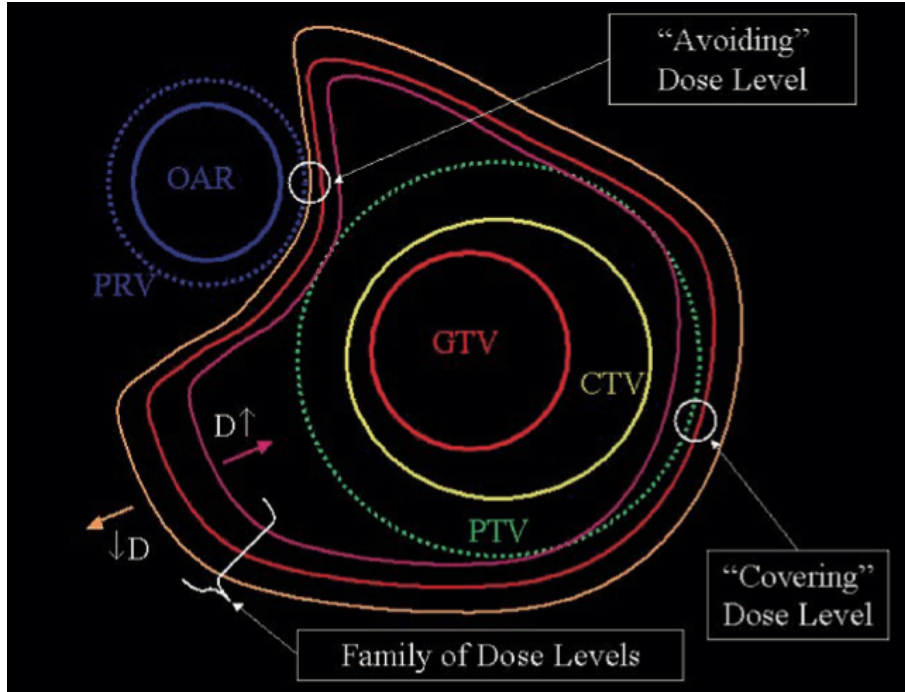


FIGURE 3.1: Illustrates the principles in designing radiotherapy plan. The figure shows the GTV, CTV and PTV volumes and the dose distribution. The figure is published by David Jaffray and Gospodarowicz [2008].

Side Effects

The side effects are highly dependent on the body region and the amount of affected tissue. Normally the side effects are categorized as general or local. The general side effects are: Fatigue, anorexia (low appetite), weight loss and nausea. The local side effects varies dependent on the local organ however, common local side effects are e. g. skin reactions and pain. Healthy tissue cannot entirely be spared in the radiation delivery. However, if the exposure is kept on a minimal level the tissue will be able to repair itself.[Coleman and Halperin, 2006; Rørth and Hansen, 2009] For each organ in the body there exist information on tolerance dosage, and normally the exposure to the organ do not reach this tolerance dosage. The aim is to kill the cancerous cells as a whole that always provides a risk of late damage to the organs. It is possible to repair late damage with surgery to some extent and is included in the basis of deciding the CTV.[Coleman and Halperin, 2006]

Medical Imaging

In conventional radiotherapy images are used in many steps of the procedure such as cancer staging, immobilisation, treatment planning, post planning verification, treatment delivery and more [Huntzinger et al., 2006]. Medical images visualise shape, structure and size in the body tissue and provide information of the spatial relationships within the body. The improvement within medical images is the foundation of more sophisticated approaches within radiotherapy e. g. the use of Image Guided Radiotherapy(IGRT), which will be described later.

Among the image modalities used in cancer diagnostics and treatments are: Computed Tomography (CT), Magnetic Resonance Imaging (MRI), Positron Emission Tomography (PET), Ultra-

sound (US) and Single Positron Emission Computed Tomography (SPECT). CT is the dominating modality in the radiotherapy due to image quality and cost.

Computed Tomography

A CT scanner system has an x-ray generator and detector mounted on a gantry that rotates around the patient. Rotating the gantry around the patient and obtaining a projection in a fixed number of angles capture the images. After a sufficient number of projections, no less than 180 degrees rotation, the images are merged by a mathematical reconstruction method that produces 3D axial slices of the patient. Today a full image of the torso can be obtained in a few seconds.[Wong, 2008].

3.2 Image Guided Radiotherapy

IGRT is a technique that uses frequent captured images to guide the treatment throughout the course of radiation delivery. In IGRT the imaging modality is connected to the radiation equipment and captures images before or during delivery, which makes the physician capable of adjustments and corrections due to patient immobilization, treatment planning, verification and correction of patient setup, and delivery of radiation.[radiologyinfo, 2011] This has many beneficial effects such as more precise and accurate detections of tissue volumes and evaluation of the treatment. IGRT is mainly used in treatment cases where the target areas are prone to movement or close to critical areas e. g. prostate gland and areas affected by the breathing cycle. In conjunction with Intensity Modulated Radiotherapy (IMRT) the quality of the radiotherapy can be more sophisticated and improve the outcome of the treatment.[radiologyinfo, 2011]

Intensity Modulated Radiotherapy

Intensity Modulated Radiotherapy is a more advanced radiation delivery method compared to the 3D conformal radiotherapy(3DCRT), which deliver radiation dosage in a uniform delivery scheme. Today IMRT is used widely on oncology centres.[De Neve, 2006]

With IMRT the treatment planner can design the dose distribution as a function of an irregular shape outlined by the PTV and OAR. This enable a more conform irradiation of the target volume, thereby minimising the damage of adjacent normal tissue.

By considering cases where the malign tissue is wrapped around OAR e. g. lymph nodes around rectum or prostate, the IMRT fully has advantages that spare the OAR. Figure 3.2 illustrates the difference between 3DCRT and IMRT. In this case IMRT is a generalization of 3DCRT with the ability to construct no uniform radiation pattern that fits the CTV.[De Neve, 2006; Mohan and Bortfeld, 2006]

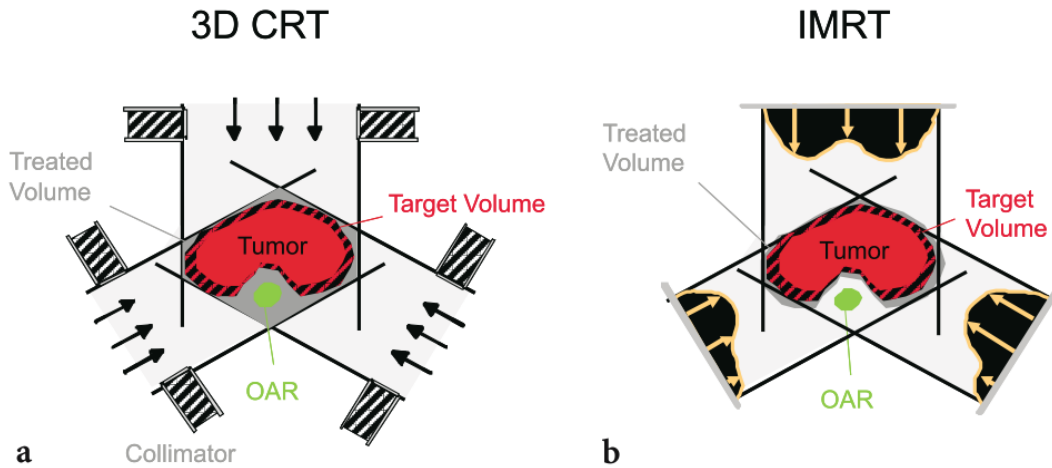


FIGURE 3.2: The principles of 3DCRT and IMRT are shown in 'a' and 'b' respectively. The 3DCRT case illustrates that the uniform distribution is unable to distinguish between the PTV and OAR, while the IMRT case can minimise the dose to the OAR. The figure is published by Mohan and Bortfeld [2006].

3.3 The Challenge of Lymph Node Delineation

As stated previously lymph nodes are an important determinant of prognosis and must be included in the clinical target volume to benefit from IMRT. Besides primary tumor and adjacent lymph tissue with microscopic disease, any enlarged lymph node and organ drainage regions with risk of containing metastasis must also be included[Cefaro et al., 2008].

The planning of target volumes includes a variety of trade offs due to the clinical objective, technical availability, efficiency and manpower. The current technology still relies on the experience and judgement of the radiation oncologist, which requires a highly-specialized competence to secure optimal treatments[Cefaro et al., 2008]. Inter-observe discrepancies arise during node delineation and may cause inconsistent CTV detection. This stresses the need of more sophisticated tools to improve and secure consistent lymph node detection.[Lengel  and Scalliet, 2009]

The introduction of IMRT has provided a huge potential to improve the treatment in terms of the precision and accuracy in the radiation delivery. However, the complexity of treatment planning and verification has increased at the same time and leads to a more time consuming treatment planning process[Schwarz, 2009]. To reduce the complexity of treatment planning for IMRT software tools could be a solution however, the quality of lymph node detection still mainly rely on the quality of the planning image. CT is dominant in terms of planning radiotherapy. However small lymph nodes are very difficult to detect on CT images and may cause inadequate cancerous tissue coverage. Reasons may be the lack of objective descriptions of the lymph nodes in 3D, which makes treatment planning difficult [Dinniwell et al., 2009]. This has motivated guideline publications to improve the detection of lymph nodes [Taylor et al., 2005; Lengel  and Scalliet, 2009].

With the currently available images it is a challenge to develop an algorithm that provides a consistent guideline to detect lymph nodes with risk of metastasis, and reduce the complexity of treatment planning.

Chapter 4

The Arteries as Surrogate

In this chapter the rationale to use arteries as surrogate to detect lymph nodes is presented. First the lymph nodes of interest are described and a guideline to find lymph nodes is presented. Afterwards a brief anatomical description of the big pelvic arteries is presented.

4.1 Lymph Nodes of Interest

The smallest lymphatic vessels are the lymphatic capillaries, which offer little resistance to cancer cell passage. Therefore the common site of spread of metastasising cancer cells is through the lymphatic vessels and end up in connections with to the veins. Along the bigger lymphatic vessels are several lymph nodes, which lie adjacent to the bigger arteries. By irradiating the pathological lymph nodes along the lymphatic drainage path, further spreading can be avoided.[Martini, 2006b] When the lymph node exceeds a size of 10 mm (short axis) or is tested positive with biopsy, the lymph node is considered pathological and must be included in the CTV. Those lymph nodes with high risk of metastasizing cell but without a visible appearance on CT are desirable to be included otherwise.

By following clinical guidelines e. g. the one published by Taylor et al. [2007] the big arteries in the pelvic are used to localise the lymph nodes as an anatomical landmark. The rationale is that the drainage from the different pelvic organs leads to these passages and has high risk of including metastasising cells depending on tumor origin. Thus lymph nodes located along the lymphatic drainage passage, which lie adjacent to artery vessels, are of clinical interest.

Lengel  and Scalliet [2009] has published a review study of lymph node areas in the pelvic region, which describes the functional drainage pathways in three main and five accessory drainage routes. Every pelvic organs has a dedicated lymphatic plexus that finally are connected with several of the eight drainage pathways. Normally the spread of different organ cancer involve at least two of the main pathways and an accessory pathway e. g. the lymphatic metastatic from uterine carcinomas may involves up to six of the pathways.[Lengel  and Scalliet, 2009]

The main pathways is located along the big artery vessels such as the common, internal and external iliac, which are relative easy to visualise on CT images. However, when cancer is diagnosed the metastasis progression may be far more complex due to several pathway usage. Therefore all efferent organ arteries are ideally of interest.

The approach to use arteries as surrogate has been studied on gynaecologic malignancies [Chao and Lin, 2002], Cervical Cancer [Uno et al., 2009], Uterine Cervical Cancer [Japan Clinical Oncology Group et al., 2010], prostate cancer [Michalski et al., 2010] and Taylor et al. [2007] has showed in several work, that the vessel margin is a suitable surrogate to detect lymph nodes in the pelvic area [Taylor et al., 2005, 2007; Vilarino-Varela et al., 2008].

Taylor et al. [2007] use a 7 mm margin to the big vessels as an initial step in a cascade of guideline steps, wherefrom the margin is expanded further if necessary. The guideline is presented in table 4.1. The guideline has shown promising results by including up to 99.5% of detected lymph node [Vilarino-Varela et al., 2008]. However, if more branches of pelvic arteries could be automatic segmented the target arteries with an margin could include even more lymph nodes to the CTV, especially those not detectable by the radiologist.

Table 1 – Summary of the guidelines for delineating nodal regions

Lymph node group	Recommended margins*
Common iliac	7 mm margin around vessels. Extend posterior and lateral borders to psoas and vertebral body
External iliac	7 mm margin around vessels. Extend anterior border by a further 10 mm anterolaterally along the iliopsoas muscle to include the lateral external iliac nodes
Internal iliac	7 mm margin around vessels. Extend lateral borders to pelvic side wall
Obturator	Join external and internal iliac regions with a 17 mm wide strip along the pelvic side wall
Pre-sacral	Subaortic: 10 mm strip over anterior sacrum Mesorectal: cover entire mesorectal space

*Also include any visible nodes.

TABLE 4.1: Summary of the guideline to delineate the lymph nodes in the pelvic area. The table is published by Taylor et al. [2007].

4.2 Pelvic Arteries

The artery vessels in the pelvic region have a tree like structure that descent from the abdominal aorta and divide into the right- and left common iliac, middle sacral and inferior mesenteric artery. Each common iliac artery divides into the internal iliac and external iliac artery.

The geometric vessel size is an important aspect in order to visually localise the vessels on a CT. Since CT images are captured with an limited spatial resolutions, vessel cross-sections below the voxel size are not detectable in the image. Depending on age, gender, body size and body region the cross sections varies. In general the Aorta is estimated to 26 mm, greater arteries to 8 mm and arterial branches range between 3-0.6 mm [A. Despopulos, 1998].

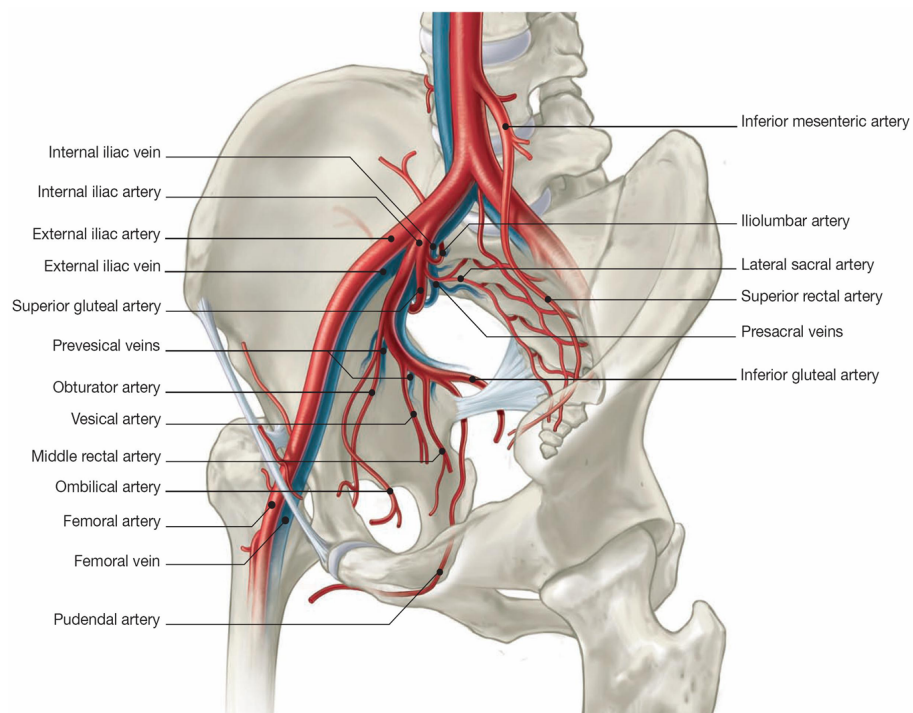


FIGURE 4.1: *Illustrates the arteries in the pelvic region. By following the guideline by Taylor et al. [2007] the lymph nodes of interest is found by locating the common, internal and external iliac artery and the smaller arteries such as the obturator and pre-sacral arteries. This figure is published by Geeraerts et al. [2007]*

Chapter 5

Problem Statement

The mortality of cancer is increasing in Denmark, and has an impact on the length and quality of life. Approximately 30% of diagnosed cancers are located in the pelvic region, which is a complex area to treat when the cancer is spreading to the lymphatic system. Cancer progression in the lymphatic system is an important factor in terms of prognosis, and by an efficient treatment in an earlier stage the outcome may improve. A conventional treatment of lymph nodes is radiotherapy and is the preferred treatment in the pelvic region. The aim of radiotherapy is to irradiate the cancer tissue as a whole and spare the healthy tissue. However, the treatment impose healthy tissue damage which is correlated to the severity of side effects.

IGRT in conjunction with IMRT is an advanced technique to perform a precise and accurate irradiation pattern and may reduce the amount of healthy tissue damage. Since IMRT is becoming a standard in the radiotherapy more experience has been obtained and several work has been published to establish guidelines and consensus in the radiotherapy. One approach in the guidelines is to recognise the lymph nodes are located adjacent to pelvic arteries and are an appropriate surrogate to detect lymph nodes with poor visual appearance. However, delineation of CTV is time consuming and has inter-variability among clinicians [Huntzinger et al., 2006]. Especially lymph nodes are difficult to delineate in medical images and may cause inclusion of healthy tissue in the CTV to ensure a confident irradiation.

One solution to improve the delineation process is to develop an image segmentation algorithm that precisely track the vessels in vessel enhanced modalities and delineate lymph nodes by applying a margin to the arteries. For instance a 7mm around the big arteries has been proposed in a guideline by Taylor et al. [2007](See table 4.1).

The source of cancer spreading is often related to the lymphatic vessels collocated with afferent organ arteries, which concern finer artery branches. By the time of cancer diagnosis the detection of pathways including metastasis may provide a more selective and comprehensive coverage with radiotherapy. Thus the artery of interest will also concern finer artery branches. However, depending on the image modality and image quality a detectable size of vessel cross section varies.

Today the radiotherapy planning is mainly performed manually by labelling CT images with CTV, which is time consuming, lack of consistency and depending on the clinicians competence. An automatic approach to determine CTV may provide beneficial effects in the radiotherapy treatment. Thus the scope is to develop a segmentation method that extracts artery branches.

The Aim of This Work

The aim of this work is to develop an image segmentation method to extract artery vessels in the pelvic region.

Part II

Analysis

Chapter 6

Research in Vessel Segmentation

In this chapter the current research and topics within vessel segmentation are introduced and provides the basis of the method design in the next part of the report. In the first section image features are introduced. In the next section a brief overview of extraction schemes is described. The benefit of vessel segmentation can be used in a variety of applications and has motivated an extensive amount of research that provides segmentation frameworks with automatic and semi automatic approaches. Lesage et al. [2009] has published a review of segmentation techniques with focus on vessel lumen, which provides a comprehensive overview of the current research. This review has been the primary inspiration to the following section content.

6.1 Image Features

An image feature is defined as an image measure to detect or filter an objective of interest, in this work the vessel lumen. The image features used in algorithm design are often based on common image analysis such as intensities and edge detectors described in handbooks.[Gonzalez, 2008] By combining these basic tools with a prior assumption on a vessel model, more advanced image features can be extracted in the image.

One common feature in vessel enhanced images relies on a isotropic intensities within the vessel and assume darker nearby structures. An illustrative work by Vasilevskiy and Siddiqi [2002] uses the spherical flux of image gradients to estimate the divergence through a spherical boundary. This approach is performed in multiple scale spaces and produce high responses in isotropic vessels. This feature however, does not consider vessel direction.

A common method to investigate vessel patterns and direction is the use of derivative features. Especially second order derivatives are able to derive curvature information and namely the Hessian matrix is used in several applications. The work by Frangi et al. [1998] were the first to introduce an intuitive model interpretation of the Hessian matrix that distinguish between plate, blob and tubular structures and was later elaborated by Lin [2003].

Florin et al. [2005] rely on several vessel appearance models to drive a particle filter. The approach is to evaluate a state vector based on an initial segmented volume and wherefrom the next state of the vessel is predicted. Among the evaluated features are vessel location, tangent vector, vessel intensity distribution and an elliptic shape model to estimate 2D cross sections.

A feature different from the others is the use of contrary features to detect non vessel structures. An example is to detect bone structure based on a spatial difference between none structures and

vessels[Felkel et al., 2001].

6.2 Extraction Schemes

In this section the concepts of extraction schemes is presented. The classification of extraction schemes is different among authors due to the extensive research and composite method schemes. Kirbas and Quek [2004] divides the extraction schemes in six categories including subcategories e. g. pattern recognition, model based approaches, tracking based etc. Suri et al. [2002] divides the segmentation approaches in skeleton-based and non skeleton based methods as a indirect or direct approach respectively. Lesage et al. [2009] classifies the extraction schemes into three groups: region growing, active contour and centerline-based methods, which are adapted in this overview. The scope of this section is to present some of the general concepts within vessel extraction. For comprehensive reading the reviews by Lesage et al. [2009], Kirbas and Quek [2004] and Suri et al. [2002] are recommended.

Region Growing

The basic region growing uses value similarity and spatial proximity to extract vessel volume. Region growing investigate neighbour points and incrementally increase the segmented volume when the neighbouring points fulfilled inclusion criteria. The approach is based on a seed point, which initialises the segmented area and process the data voxel wise. The main advantage of region grow is the simplicity, computational efficiency and the segmented volume is a connected structure.[Gonzalez, 2008]

A classic example of inclusion criteria is an intensity thresholds which Boskamp et al. [2004] uses to obtain an initial segmentation. The downfalls however, are the risks of false negative and false positive since the criteria is sensitive to noise and inhomogeneous contrast agents in the vessels.

Active Contour

The active contour approach evaluates two forces, the external forces based on the image features and internal force based on a model to constrain and design the contour property. The forces act as an interface to extract vessel contours by minimizing an energy function.

The classical active contour is based on parametric active contours also known as snakes, which is based on a Lagrangian formulation of curvature evaluation[KASS et al., 1987]. The downfall of parametric active contour is the lack of capability to incorporate topology changes. However further development has lead to topology adaptive active snakes that encounter splitting and merging of contour features and is considered an advantages in complex medical structures [McInerney and Terzopoulos, 2000]. Implicit active contour is a technique to extract a contour implicitly. Today this has become conventional known as the level set method, which evaluates the active contour based on a Eulerian formulation. In contrary to parametric active contour that evaluate a initialised number of particles, the level set method implicitly handle topology changes by evolving an interface function defined in the entire image. This method however increases the computational cost and the developer must ensure convergence. An illustrative work is 'Curves' by Lorigo et al. [2001], which reduce a 3d evaluation problem to 1D and is well adapted to vascular structure.

In general the active contour method is flexible in the sense that it allows internal and external

force design in many variations. The parametric active contour has an efficiency advantage and is well suited for interaction and open contour in contrary to implicit active contour. However for more complex structures the implicit active contour benefits from implicit topology adaption.

Centerline-Based Methods

The centerline-based approaches extract the centerline of the vessel instead of vessel lumen, thus to extract the vessel lumen an extra processing step is required.

One method is the direct centerline tracking method, which normally is semiautomatic requires initialising seed points. The vessel branches are tracked separately with a manual selection of seed points from which the centerline is tracked iteratively with prediction and correction steps. An example is a direct centerline tracking approach by Wink et al. [2000], which track a centerline voxel in every iteration based on previous estimated center likelihood and vessel axis. Various approaches are suggested to perform robust estimations of vessel direction such as incorporating geometric feature models. However, the approach is still prone to image abnormalities and requires manual interaction. The methods is suitable for large 3D data due to sparse exploration of data and relative low memory requirements.[Lesage et al., 2009]

The minimal path technique is an approach based on a start and end point. In between these points the minimal path is tracked according to an cost metric based on selected vessel-dedicated features. An example is a work by Olabarriaga et al. [2003], which use the reciprocal of a vessel enhanced image to evaluate the minimum cost between two points. The techniques differ in the sense of employed numerical optimization schemes and classical issues is concerned with erroneous shortcuts when minimizing the cost path.

Chapter 7

Data Analysis

In this chapter is an analysis of the data used in this work presented. The focus of the analysis is to evaluate the vessel appearance in the data to make assumption on the vessels in the method design.

7.1 The Data

In this work the data used to develop a segmentation method is based on CT angiography (CTA), which enhance the arteries in the pelvic region. To obtain arterial enhancement a intravenous contrast bolus is administrated prior to CT image acquisition with a preset region of interest. The quality of the arterial appearance is dependent on factor such as operator assessment, patient cardiac output, body habitus etc. However, some of the of the most important factors are controlled by the operator and includes scan timing, contrast volume and contrast concentration etc.

The data in this work is captured by administrating the contrast Iomeron or Omnipaque and uses a scan timing technique called bolus tracking. This technique relies on an automatic peak detection of contrast flow in the pelvic region. After the injection of contrast the scanner is triggered when the pelvic region obtains a peak in contrast concentration. The aim is to use a time delay that maximise the amount of contrast when the CT scanner is initialised. In this work the region of interest is the aorta, in which the peak of contrast is tracked and automatically activates the CT scanner. [Carl, 2011; Kirsch et al., 2007].

The datasets is captured from fourteen patients in the age ranging from 60 to 80 years old. All patients have diagnosed rectum or rectal cancer. The data is allocated in 12 bit with intensities ranging from 0 to 4095, and has an spatial resolution of $1 \times 1 \times 2.5 \text{mm}^3$ in a voxel.

7.2 Vessel Appearance

. The intensities in the CTA data are represented in Hounsfield units (HU), which is a standardisation to calibrate the intensities. Since the data is 12 bit, the images provides an intensity range of -1024 to 3071 HU corresponding to 0 to 4095 digitally in the data sets. In table 7.1 the intensities are presented according to the structure in the image.[Wikiradiography, 2011]

Since the amount of contrast, contrast type and scanning time delay varies the intensity varies among data sets. Thus the intensities of arteries are difficult to determine and requires a further analysis of the images to.

Structure	Intensity	HU
Air	0	-1024
Fat	924 to 974	-50 to -100
Water	1024	0
Muscle	1034 to 1064	10 to 40
Kidney	1054	30
Blood	1064	40
Bone	1260 to 2024	1000

TABLE 7.1: *Presents different image structures with corresponding image intensities.[Wikiradiography, 2011].*

To investigate the intensities in the image histograms are presented in figure 7.1. The upper left image shows a transversal CTA image of the pelvic containing a region '1' corresponding to the aorta and region '2' corresponding to a spine structure.

The upper right figure shows a histogram of the entire CTA image, which contains three peaks. The first peak is located near zero intensity and correspond to air structure or very low density structures. The second peak is located in the near 950, which correspond to fat. The third and last peak is located near 1050 and has a right flattering shape. The intensities in the peak area include muscle, kidney blood and water, whereas the flattering part mainly consists of bone. Note the overlapping spectrum between the second and third peak which are related to different variations within the structure e. g. spongy bone have lower density compared to compact bone.

The lower left of the figure shows a histogram of the region '1', which has a peak around 1340. The histogram illustrates the enhanced aorta intensities.

The lower right of the figure shows a histogram of region '2' and has a peak around 1200. The shape is flattering to the right just like the bone spectrum. However, the shape illustrates that the spongy bone dominates the spectrum in the lower intensity spectrum, while the relative small appearances of compact bone at the border are located in the higher spectrum.

One of the main challenge in the data sets are to distinguish enhanced vessel structures and bone [Felkel et al., 2001]. Figure 7.2 presents a case where the vessel structures approaches bone structure and is located closely nearby the bone. This case illustrates the course of the internal iliac artery which later e. g. divides into lateral sacral artery and iliolumbar artery(See anatomy in Figure 4.1).

Figure 7.3 in upper left corner shows an image of the blood vessel, bone and muscle tissue structure. The blood vessel and bone in the intermediate spectrum tend to have similar intensity and can not be distinguished by analyzing the intensity alone. The right image shows the aorta with calcification.

A common assumption within CTA is the intensity increases as the centerline of the vessel is approached. The assumption is based on the laminar flow peaks near the center of the vessel and thereby obtains higher contrast flow. In contrary the laminar flow near the vessel border is reduced due to friction.[A. Despopulos, 1998]

As described in section 4.2 the vessels in pelvic has a tree like structure ascending from aorta. The shape of the vessel has a tube like structure with largest cross section diameter in aorta and decrease in size through down the vessel tree. Several factors cause the vessel to change from a tube to a more complex structure such as bifurcation and anomalies. Bifurcations occur in every

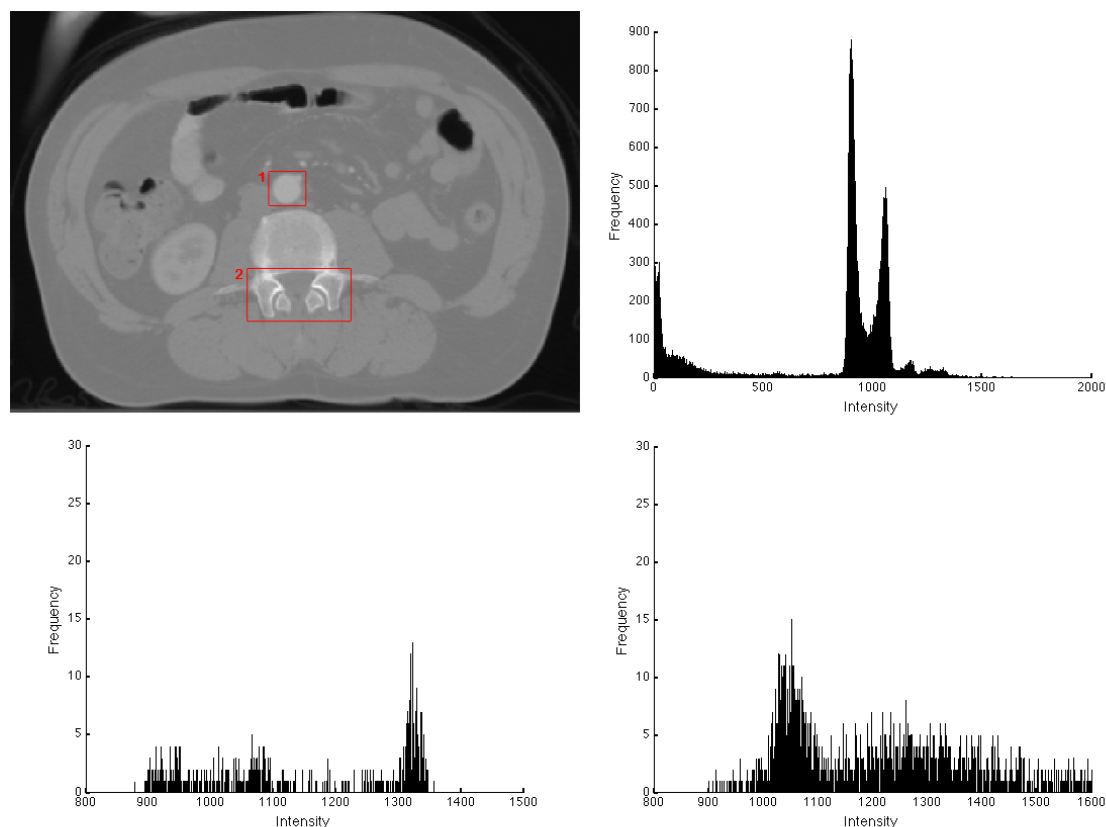


FIGURE 7.1: Illustrates the intensity spectrum in different structures. The upper left figure shows a transversal slice from CTA data. The upper right figure shows a histogram of the entire intensity spectrum based on the CTA image to the left. The lower left and right figure illustrates the histogram for the aorta structure in region '1' and spine structure in region '2' respectively.

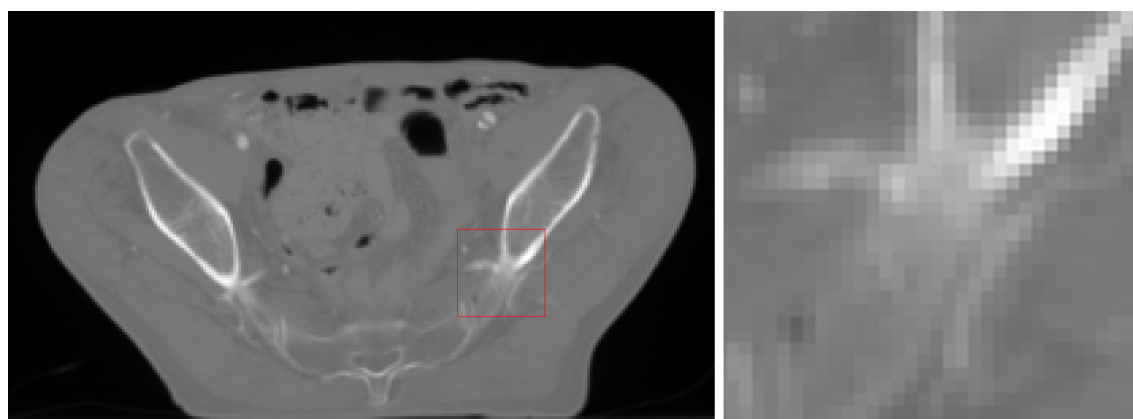


FIGURE 7.2: Illustrates the overlapping visual appearance of enhanced vessel and bone structure. The left Image shows a CTA image in the transversal plane and the right image shows the magnified region marked with red colour in the transversal CTA image.

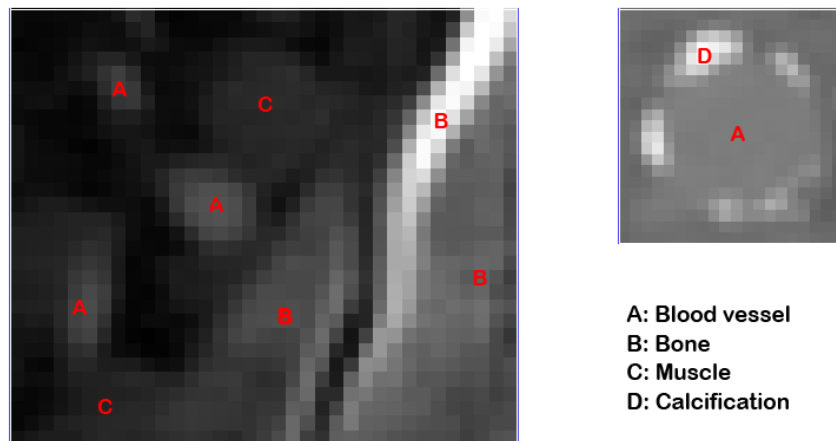


FIGURE 7.3: Shows the visual appearance of different closely located structures. The left image shows three structures: Bone, blood vessel and muscle. The right image shows a visual appearance of aorta containing classification.

branch of vessel tree and anomalies such as calcifications, aneurysms, stents and stenosis causes a very complex structure of the vessel tree.

To illustrate the tree structure Figure 7.4 shows a rendered volume of one data set. The figure shows the bone structure and vessels is located close nearby both spatially and intensity wise. Note that the aorta is located in the top of the image and has a different intensity compared to the vessels in the bottom of the images. This can be explained by reduced contrast due to laminar flow and an inconsistent bolus CT tracking technique.

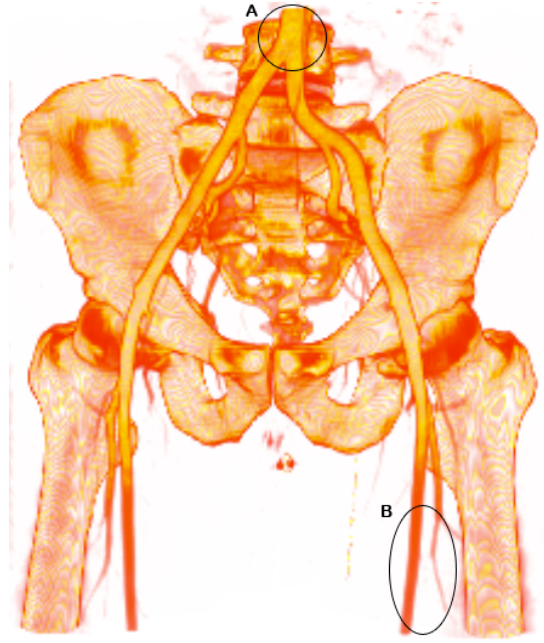


FIGURE 7.4: Illustrates a rendered volume of data set 14. The left image shows a the linear colour in the intensity interval 1100 to 1350. A) Location of Aorta. B) Area of femoral artery in the bottom of the vessel tree.

7.3 Artefacts

An artefact is a visual image feature that does not correspond to an object under investigation. Typically an artefacts is caused by a defect image reconstruction and amplified structures causing greater and visual prominent appearance compared to random noise. An reconstruction error is an deviation in values within the same material though in different locations.[Karen M. Mudry and Bronzino, 2003] Within the CTA images an artefact arises when metallic objects is worn by the patient such as watches and rings inside the CT scanner. Also Internal objects such as prostheses affects the imaging of the tissue. The object may produce noise in adjacent image structure and thereby affects the image gradient.

In the segmentation algorithm artefacts such as a prosthesis must be taken into account to avoid misinterpretation from the clinician. However, in practice some amount of reconstruction errors and noise must be tolerated due to the conventional reconstruction methods and equipment.

The partial volume effect (PVE) is the CT equipment inability to image body volumes in a coarse resolution. Since integrating radiation signal in a resolution matrix generates the image, the voxel intensities are an average of body tissue in the voxel volume. Thus the voxel intensity is a representation of the dominant tissue in the voxel volume.[Cunningham and Judy, 1999]

Small arteries are especially affected by PVE and complicate the detection. However, by increasing the resolution the PVE is reduced and may improve segmentation of smaller vessels. The fourteen data set in this work has a anisotropic resolution with 2.5 mm in the transversal plane compared to 1 mm in the other two planes. This causes an increase of the PVE in the transversal plane. PVE may not be considered an artefact, but rather compared to noise, which affects the quality of the image data.[Karen M. Mudry and Bronzino, 2003]

Part III

Method

Chapter 8

Applied Segmentation Method

In this chapter the developed segmentation method is described. To extract vessels in CTA data a segmentation method rely on underlying assumptions made on vessels and vessel appearance. To incorporate the assumptions into a segmentation algorithm a number of suitable image features are selected to drive the extraction scheme. In the first section the applied method will be introduced by describing the made assumption on a vessel. Based on the made assumptions the segmentation approaches is selected which will be presented in the method introduction.

In the second section a brief description of the entire method is presented to provide an overview of the segmentation method.

8.1 Method Introduction

In this section the developed segmentation method is introduced. The scope will be a semiautomatic approach that can support a radiologist to determine detailed IMRT margins (see section 4.1).

Based on the data analysis in the previous chapter and research the following assumptions are made:

1. Vessels have enhanced intensities compared to the close surrounding tissue.
2. Within vessel lumen the intensities are similar throughout the branches.
3. Vessels are defined within a specific intensity range.
4. Vessels are connected in a tree like structure.
5. Vessels have a tube like shape.
6. Bone has larger volumes compared to vessels.

Assumption one and two are made based on the technique of using contrast to enhance vessels and thereby appear brighter. The third assumption is partial valid since smaller vessels does not have the same flow as bigger vessels and have overlapping intensity spectrum with bone. However, in the method design the segmentation is limited to vessel segmentation based on the contrast enhanced vessels.

The fourth and fifth assumption is made to consider a geometric model of a vessel. Assumption four is based on anatomical knowledge and does not consider abnormalities such as aneurysm etc. The fifth assumption is based on a circular cross section model that together constitute a tube

structure elongated throughout the branches. The last assumption is considered to separate the bone structure from the vessels and is not an assumption on vessels alone.

Method Selection

One of the main challenges in pelvic vessel segmentation is to separate image objects with overlapping intensity spectrum in CTA data. Therefore a simple threshold of CTA data will extract other tissue and structures than enhanced vessels. Instead the selected approach is to use a method that in steps use the before mentioned assumptions and find reasonable features to extract vessels.

A common assumption within vessel segmentation is that the vessel lumen has similar intensities throughout the vessel branches. In CTA data vessels have a brighter intensity compared to the surroundings and thereby provide a relative clear distinguishable appearance. The combination of similar intensities within vessel lumen and enhanced vessel intensities suggest a region growing method, which is a common semiautomatic method.

Region growing is a relative simple method that extracts a connected structure such as a vessel tree and depends on a seed point selection. In reality a vessel may be disconnected due to e.g. noise or stenosis, thus some vessel branches may be omitted and cause a limited extracted volume. Bone structure and enhanced vessel structure have an overlapping spectrum and complicates the segmentation. An approach is to remove bone structure before vessel segmentation. One suggested method is to use a threshold followed by morphological operation and connected component [Felkel et al., 2001]. Another approach is to simply perform a manual pre masking of the image [Boskamp et al., 2004]. In this work however, the bone structure is removed by adapting an automatic bone filter by Yang and Holch [2010], which use a preset intensity and spatial threshold.

To find disconnected vessel branches this work develops an extension to a region growing method, which uses tubular like feature structures in a vessel. The extension is adapted from a thesis by Graham [2008] and later published by Graham et al. [2010]. The method uses a five stage segmentation approach on multi detector CT (MDCT) data to extract lung airways and were developed with the purpose of image-guided peripheral bronchoscopy.

The first stage uses a conservative volume of the bronchi tree extracted with a simple region growing method. Stage two uses a nonlinear filter to extract 2D elliptic cross section based on the assumption that the periphery airways have a lower intensity compared to the nearby voxels. Stage 3 uses adjacent 2D cross section to establish sequences of tube segments most likely to represent an airway. Stage 4 creates a preliminary connection between the conservative bronchi tree and the sequences of segments. In addition the remaining segments are graded and represented in a graph. Stage 5. uses a graph optimization scheme to extract the final segmentation.

This work adapts stage 2 and 3 by Graham et al. [2010] that approximate bronchi cross sections with an ellipsis and later creates a tube like model to extract the bronchi airways. Based on the CTA data analysis in previous chapter and shape knowledge of the airways bronchia, pelvic vessels are assumed to have similar characteristics. In addition previous work has used an ellipsis approximation on vessels [Florin et al., 2005], which justifies a cross section approximation to vessel structure. However the intensity spectrum of vessel lumen in CTA is different from airways bronchia in MDCT images, thus the method needs adaption to vessel intensities in CTA data.

8.2 Overview of the Segmentation Method

In this section the overview of the complete segmentation method is presented. The segmentation method is illustrated in Figure 8.1 and has the following stages:

1. stage extracts the big vessel with a region growing algorithm. The purpose is to extract big vessels such as the aorta and common iliac vessels (The anatomy is described in section 4.2). This stage requires a manual selection of a seed point to initialise the region growing. In this stage a bone filter is applied and modified with the initial extracted vessel tree.
2. stage contains the adapted stage 2 and 3 by Graham et al. [2010]. First step performs a filtering scan to extract 2D elliptic cross-sections in the transversal, sagittal and coronal plane and later refines the cross sections in 3D. The next step estimates surfaces between the cross section to constrain a region growing method between two cross sections. The scope is to extract tube like structures that likely model a vessel in the CTA data. This step produces a number of segments that consist of a sequence of connected cross sections and voxel lumen.
3. stage connects the vessel tree from stage 1 and vessel segments from stage 3. The approach is to use the extracted segments as seed points and apply a region growing method to establish linkage between segments and initial vessel tree.

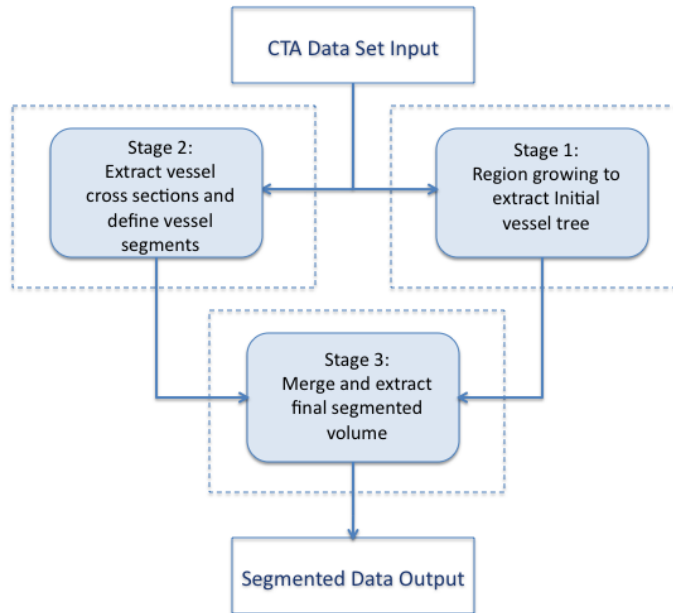


FIGURE 8.1: Illustrates the entire segmentation method. The input is CTA data and used in the two first stages. The 3. stage uses the results from stage one and two to extract the final volume.

Chapter 9

Stage 1: Initial Segmentation

The purpose of stage 1 is to produce an initial segmentation of the vessels tree including the big vessels in the pelvic region. The extraction schema is region growing and has the advantage of simplicity and ensures a connected volume. To initialise the region growing one seed point is placed within aorta. From the seed point the region growing propagate according to threshold interval to a mean intensity. The region growing continues with a increasing threshold until a preset maximum voxel count is included. Based on the reached threshold a more conservative threshold is selected as the final threshold.

Seed Point Selection

The initial seed point is placed in the aorta, which is the root to the entire vessel tree in the pelvic region. The selection of seed point is performed with an investigating of the first transversal slice in a CTA dataset. The appearance of aorta has a bright lumen due to the contrast modality, and has several characteristics such as a relative large diameter with approximately 20 mm, circular cross section and located in the middle of the transversal plane (The most proximal slice). Figure 7.1 in section 7.2 shows an image with aorta marked with a red box. The segmentation results may experience variation e. g. by selecting a seed point representing a calcification structure. However, as long the seed point is placed within the aorta lumen, the difference in extracted volume is tolerated to some extend.

Region Growing

This region growing method iteratively includes voxel adjacent to a volume if inclusion criteria are fulfilled. A traditional region growing approach e. g. use a static preset threshold or neighbourhood intensity mean as criteria for including voxels[Gonzalez, 2008]. However, as described in the analysis in section 7.2 the contrast modality and laminar flow alter the intensities throughout the vessel tree, therefore an adaptable region growing approach is appropriate. The applied region growing method is adapted from Yang and Holch [2010] and uses a global threshold criteria to include voxels. The criteria is presented in equation 9.1 where $I(x, y, z)$ is the intensity in voxel (x, y, z) , μ is the mean intensity of the already included voxels and TH is a threshold for a preset maximum absolute difference between the mean and voxel intensity.

$$|I(x, y, z) - \mu| < TH \quad (9.1)$$

The mean value is calculated according to the already included voxels and thereby adapt to vessel dedicated voxels. See equation 9.2 for mean estimation. This enables an conservative initialisation of TH, which enables adaption to a specific data set.

$$\mu_{new} = \frac{\mu_{old} + I(x, y, z)_{new}}{n + 1} \quad (9.2)$$

The number of considered adjacent voxels are determined by the connectivity to a the segmented voxel volume. In this work a 6-connected adjacent voxels is considered a conservative segmentation since this only consider the closest adjacent voxels.

The TH value is determined with an automatic approach. The TH value is initialised to zero and iteratively increased. After each iteration the voxel count in the segmented volume is investigated. When the voxel count exceeds 50000 voxels the iterations stops. The reached threshold ($TH_{reached}$) is used to estimate a conservative TH value, which ensure no over segmentation. The final TH value is calculated in equation 9.3. In this work k_{cons} is selected to 0.5.

$$TH_{auto} \approx TH_{reached} \times k_{cons} \quad (9.3)$$

Bone Filter

As described in a previous section a main challenge in the pelvic region is to separate bone from contrast enhanced vessels. Especially when the patient suffer from degenerative diseases the vessel and bone has overlapping intensity spectrum

In this work a bone filter is applied to remove bone from the data set. The approach is adapted from previous work by Yang and Holch [2010] and is illustrated in figure 9.1. The method investigates all 2D slices in the transversal plane to detect bone structures. For each transversal 2D slice a binary image is created based on a threshold to distinguish bone structures from the surroundings. Secondly all binary areas which constitute a area with a hole is filled. Thirdly a spatial threshold is used to remove binary areas larger than a preset area threshold. The biggest vessels and vessels connected to bone structure are most likely affected by the bone filter.

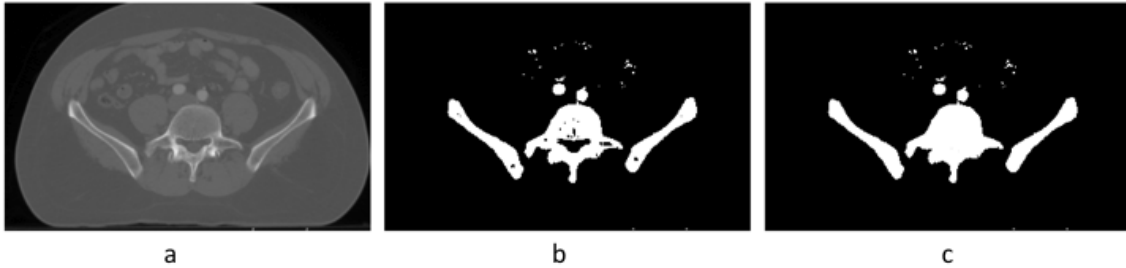


FIGURE 9.1: Illustrates the bone removal filter. a) Shows a transversal plane where the high intensities most likely constitute a bone structure. b) is the binary image of a and illustrates the large bone structure. c) Shows the hole filling of bone structure.

Ideally the bone filter should avoid all vessel, however vessels directly adjacent to bone structure is difficult to extract with a automatic segmentation method, and normally requires a manual approach. In this work minimised vessel removal caused by the bone filter is tolerated.

Formally the final bone filter is described by equation 9.4. $I(x, y, z)_{Bone}$ represents a binary image of the bone filter and $I(x, y, z)_{stage1}$ as the initial segmented vessel tree. $I(x, y, z)_{BoneFinal}$ is the final bone filter after adjustment with the initial segmented vessel tree.

Based on preliminary test and previous work by [Yang and Holch, 2010] the intensity threshold is set to 1200 and the spatial threshold is set to 200. The intensity threshold includes a large amount of vessel dedicated voxels. However most of the removed vessels are adjusted with the volume extracted the initial region growing segmentation.

$$I(x, y, z)_{BoneFinal} = I(x, y, z)_{Bone} - (I(x, y, z)_{Bone} \cap I_{stage1}) \quad (9.4)$$

Stage 1 Overview

To describe the initial segmentation the algorithm is presented in pseudo code in algorithm 1. After the vessel tree is extracted the bone filter is adjusted according equation 9.4 and applied in the extended segmentation method, which is described in the next chapter.

Algorithm 1 *Describes the initial segmentation algorithm.*

Require: Initialisation of parameters

```

1: Max Voxels=50000, TH=1,  $\mu = I(seed)$ ,  $I(seed)_{stage1} = 1$ 
2: while  $|I_{stage1}| \leq \text{Max Voxels}$  do
3:   Investigate all 6-connected neighbour voxels in volume
4:   find neighbour  $(x, y, z)_{min}$  with minimum distance to  $\mu$ 
5:   if  $|I(x, y, z)_{min} - \mu| \leq TH$  then
6:     Include  $(x, y, z)_{min}$  in volume
7:     Calculate new  $\mu$ 
8:   else
9:      $TH = TH + 1$ 
10:  end if
11: end while
12: TH=round( $TH_{reached} \times k_{cons}$ )
13: Return volume extracted with TH

```

Chapter 10

Stage 2: Extended Segmentation

In this section the extended segmentation method is described. The purpose of the extended method is to extract a pool of segments based on a tube like feature structure in the CTA data. As described in a previous section the extended method is adapted from previous work by Graham [2008]; Graham et al. [2010]. The method was original developed to bronchoscopy and constitute of five stages. However, the extended method in this work is adapted from stage two and three by Graham et al. [2010].

In the first section the method to extract cross sections is described. The approach is a filtering scan to extract a liberal amount of cross sections in 2D planes and later refine the approximation in 3D.

In the second section a pool of segments is defined based on voxel volumes between consecutive cross sections. In this process a sequence of connected cross sections are defined as a segment.

10.1 Detection of Vessel Cross Sections

In this section the method to extract cross sections is described. The approach is an approximation of a elliptic features in the image. The feature is selected under the assumption that vessel has a tube like structure and the vessel cross sections has higher intensities compared to nearby structures. The concept is illustrated in figure 10.1 and considers a local vessel branch in the transversal plane. Note that the method description uses a similar notation as Graham et al. [2010].

A vessel cross section is approximated as an ellipsis in three consecutive planes denoted as $\{A_{i-1}, A_i, A_{i+1}\}$ for the plane $z = [i-1]*\delta z, i*\delta z, [i+1]*\delta z$ respectively. Since the ideal vessel direction does not correspond to the cross section normal in the transversal plane, the eccentricity of the ellipsis deviates from a ideal circular shape(See Figure 10.1). To accommodate this a regression line is estimated between the centers of $\{A_{i-1}, A_i, A_{i+1}\}$ denoted $\{c_{i-1}, c_i, c_{i+1}\}$ from which the vessel direction \vec{n}_j is estimated. To establish a final cross section denoted B_i , $\{A_{i-1}, A_i, A_{i+1}\}$ is projected on to the plane defined with \vec{n}_j and c_j , in which the average of the ellipses is estimated. The result is an approximated elliptic cross section with center c_j and a normal \vec{n}_j pointing along the vessel direction.

The method is implemented in two steps. Step one scans the transversal, sagittal and coronal plane to detect 2D cross sections. In the second step the 2D candidates are analysed to extract a reduced amount of candidates approximated to an estimated vessel direction in 3D.

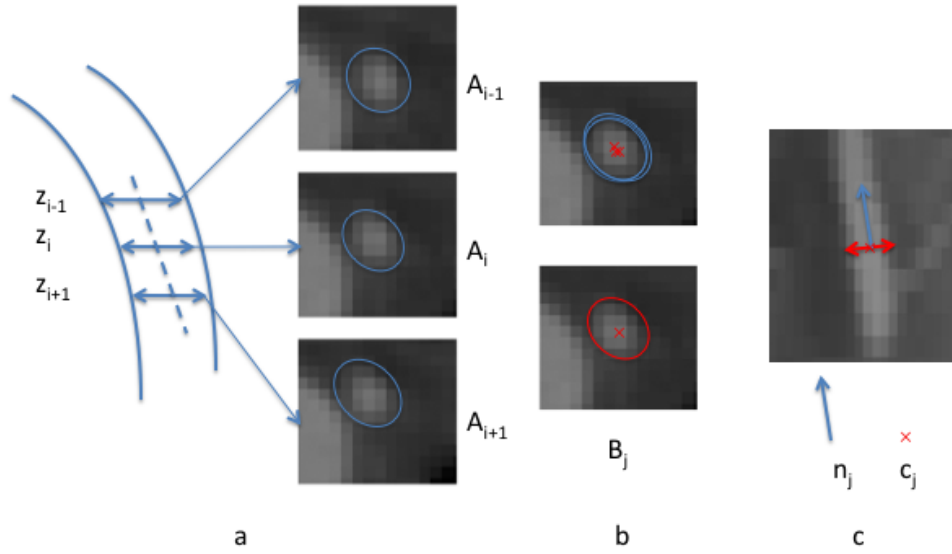


FIGURE 10.1: *Illustrates the method to approximate an elliptic vessel cross section in CTA data. a) $\{A_{i-1}, A_i, A_{i+1}\}$ are three adjacent cross sections. b) Shows the three ellipses projected on to the same plane and averaged to construct the final cross section candidate B_j . c) Shows the vessel in the sagittal plane with the cross section B_j and the vessel direction estimated with n_j . The figure is a modified figure by Graham [2008].*

Extract Cross Section Candidates

All cross section is extracted by making a scan in the transversal, sagittal and coronal plane. The method assumes that vessels have a brighter intensities compared to the nearby surroundings. The scanning is performed with thresholds to detect connected components in binary 2D images. Since the intensity appearance of vessel lumen varies due to contrast agent, vessel diameter and location, the scanning includes a wide range of thresholds, which consider the variation in vessel intensity. The intensity range is selected based on an examination of the CTA data sets. As the largest vessel with the highest contrast flow, the intensities within aorta were selected as the highest intensity threshold. The lower boundary was selected based on examination of smaller vessel with a relative bright vessel appearance. The selection of upper intensity boundary was determined based on maximum intensity within the aorta examined in slice $z=1$ in the transversal plane. The lowest intensity was selected based on the last slice in the transversal plane where smaller vessels were detected. Since the CTA data has considerable intensity variations the threshold range was selected based on empirical investigations. In this work the intensity range was selected to be 1100 to 1500 denoted $t \in [1100; 1500]$. Note that during the threshold selection vessel calcifications were not considered. However, since the image has an applied threshold the calcification will appear within the vessel, and thereby contribute to the elliptic cross section approximation.

The following description is based on a scan in the transversal plane, which is denoted as slice z_i . The scanning is performed by using thresholds in the range of t with an iteration step on ten in the plane image slice $I(:, :, z_1)$. For each threshold a 2D cross sections is located as a connected components in a binary image $I_b(:, :, z_1)$. The cross sections is denoted A_i and the boundary ∂A_i are defined as:

$$\left(\begin{array}{l} A_i = \quad 4\text{- connected voxel region for } I(:, :, z_1) \geq t \\ \partial A_i = \notin A_i \text{ and } 4\text{- connected neighbourhood voxel} \in A_i \end{array} \right)$$

In addition a score for each cross section A_i is calculated with:

$$f(A_i) = -\max_{(x,y,z_i) \in \partial A_i} + \frac{1}{|A_i|} \sum_{(x,y,z_i) \in A_i} I(x, y, z, z_i) \quad (10.1)$$

In equation 10.1 $|A_i|$ denotes the number of connected voxel in A_i . The $f(A_i)$ score provides a score on the cross section fit to a bright vessel lumen. With a high score the $f(A_i)$ is more likely to fit a vessel cross section. However, in bone structures such as the spine, a high scoring A_i may represent a piece of bone due to the high intensity in dense bone. This may contribute with a large amount of false vessel-dedicated cross section. To accommodate this the bone filter in section 9 is applied to remove a large amount of bone volume.

For each $f(A_i)$ the cross sections are approximated with a ellipsis representation given by:

$$x_i(\theta) = P^T M_i \theta + c_i \quad \theta \in [0; 2\pi] \quad (10.2)$$

The ellipsis is represented with a 2x2 matrix M_i defined in equation 10.4. (e_1, e_2) and (λ_1, λ_2) is the eigenvector and eigenvalue of the covariance matrix presented in equation 10.3. The T denotes the transpose of the matrix and the sum of x and y is for $(x, y) \in A_i$, while z_i is used as illustration in the transversal plane. The last term in equation 10.3 is to obtain a non singular matrix when A_i only contain one voxel.

$$Cov(A_i) = Cov(A_i) + \frac{1}{12} \begin{pmatrix} 1 & 0 \\ 0 & 1 \end{pmatrix} \quad (10.3)$$

In the cross sections scan two exclusion parameters compared are considered. The first exclusion parameter is a maximum area of A_i . Based on examination of an aorta cross section an area larger than 400 voxel is considered a non vessel cross section and is discarded. The second parameter is based on an estimate of the elliptic shape using the quotient of the two absolute eigen values of the covariance. The eigenvalues represent the spanning on the principle axis and with a quotient approaching zero the eccentricity increases and thereby deviate from a circular cross section. In this work 0.20 is selected as a threshold to discard cross sections with high eccentricity.

$$\begin{aligned} M_i &= 2 * \begin{bmatrix} e_1 & e_2 \end{bmatrix} * \begin{bmatrix} \sqrt{\lambda_1} & 0 \\ 0 & \sqrt{\lambda_2} \end{bmatrix} & \theta &= \begin{pmatrix} \cos\theta \\ \sin\theta \end{pmatrix} \\ c_i &= \begin{pmatrix} \frac{1}{|A_i|} \sum x \\ \frac{1}{|A_i|} \sum y \\ z1 \end{pmatrix} & P^T &= \begin{bmatrix} 1 & 0 \\ 0 & 1 \\ 0 & 0 \end{bmatrix} \end{aligned} \quad (10.4)$$

The $x_i(\theta)$ represent a parametric representation of an ellipsis projected in the x - y plane by P^T and is characterized by M_i with center c_i as a 3x1 vector. As previous described the scanning includes the sagittal plane $I(x, :, :)$, and the coronal plane $I(:, y, :)$. The result is a large amount of a cross section set $\mathbf{A} = \{A_i, \quad i = 1, 2, \dots, N_A\}$ with a cross section count N_A .

Refine Final Vessel Cross Sections

Based on the cross section set \mathbf{A} the next step is to reduce the number of candidates and refine the approximation of the cross sections. The final candidates are denoted $\mathbf{B} = \{B_j, \quad j = 1, 2, \dots, N_B\}$ and produce a final cross section count of N_B candidates with a normal vector pointing along the estimated vessel direction.

To describe this step the transversal plane is continued as example, thereby $A_i \in \mathbf{A}$ is a cross section in the x-y plane in slice z_i . To estimate the vessel direction related to A_i in c_i two cross sections in the directly adjacent planes is considered with $\{A_{i-1}, A_{i+1}\}$ in the transverse plane $I(x, y, z_{i-1})$ and (x, y, z_{i+1}) respectively. The three ellipsis are characterised by $\{M_{i-1}, c_{i-1}\}, \{M_i, c_i\}, \{M_{i+1}, c_{i+1}\}$ in the plane n_j with center c_j . If the $\{A_{i-1}, A_i, A_{i+1}\}$ overlap the center of the cross sections is likely to fit the medial centerline of a vessel, thus a reasonable vessel direction can be estimated with a regression line. If one cross section lack of overlap the considered candidate A_i is discarded as cross section candidate.

The medial axis in the vessel is estimated with a linear regression line based on the three centers $\{c_{i-1}, c_i, c_{i+1}\}$. The method use the principle axis method which provide a centroid q_i on which the resulting line passes. The formula to determine q_i is presented in equation 10.5 .

$$q_i = \frac{1}{3}(c_{i-1} + c_i + c_{i+1}) \quad (10.5)$$

The vessel running direction is denoted as \vec{n}_j , which is a 3x1 vector derived with the largest eigen value from the covariance matrix in equation 10.6.

$$M_{n_j} = \frac{1}{3} \sum_{l=i-1}^{i+1} [(c_l - q_i)(c_l - q_i)^T] \quad (10.6)$$

Based on n_j a local 3D coordinate system is applied to find a projection plane orthogonal to the running direction. With a r_i (right hand) and u_i (up) 3x1 vector orthogonal to \vec{n}_j the final cross section candidate can be estimated with equation 10.9, 10.10 and equation 10.7.

$$\begin{aligned} M_i^p &= Q(n_i) + \theta + c_i^p \\ c_i^p &= Q(n_i) * [c_i - q_i] \\ Q(n_i) &= [r_i, u_i]^T \end{aligned} \quad (10.7)$$

The ellipsis approximation is also calculated for A_{i-1} and A_{i+1} and used to calculate a measure that finds the A_{i-1} and A_{i+1} candidates with highest probability to constitute a vessel with A_i . The measure is given by equation 10.8. The median is based of the three cross section scores and the operator G, which is the area of ellipses intersection divided by the ellipses union area. The first term consider the strength of the underlying vessel appearance and the second term is to determine the level of overlap. For G approaching one the overlap and thereby the similarity of the geometric cross section is determined. For a increasing $g(A_i)$ the best model fit of intensity appearance and geometry are achieved.

$$g(A_i) = \text{median}(f(A_{i-1}), f(A_i), f(A_{i+1})) * G(A_{i-1}, A_i, A_{i+1}) \quad (10.8)$$

The final cross section construction of B_j is obtained with the A_{i-1} and A_{i+1} pair that provides the highest $g(A_i)$ score. The cross section representation is given by equation 10.9 and 10.10. $\{M_j, c^p\}$

is the average 2D ellipsis characterized by: $\{M_{i-1}^p, ci - 1^p\}, \{M_i^p, ci^p\}, \{M_{i+1}^p, ci + 1^p\}$. The final cross section representation of B_j is characterised by: $\{n_j, Q(n_j), M_j c_j\}$.

$$x_j(\theta) = Q^T(n_j)M_j\theta + c_j \quad (10.9)$$

$$c_j = Q^T(n_j)c^p \quad (10.10)$$

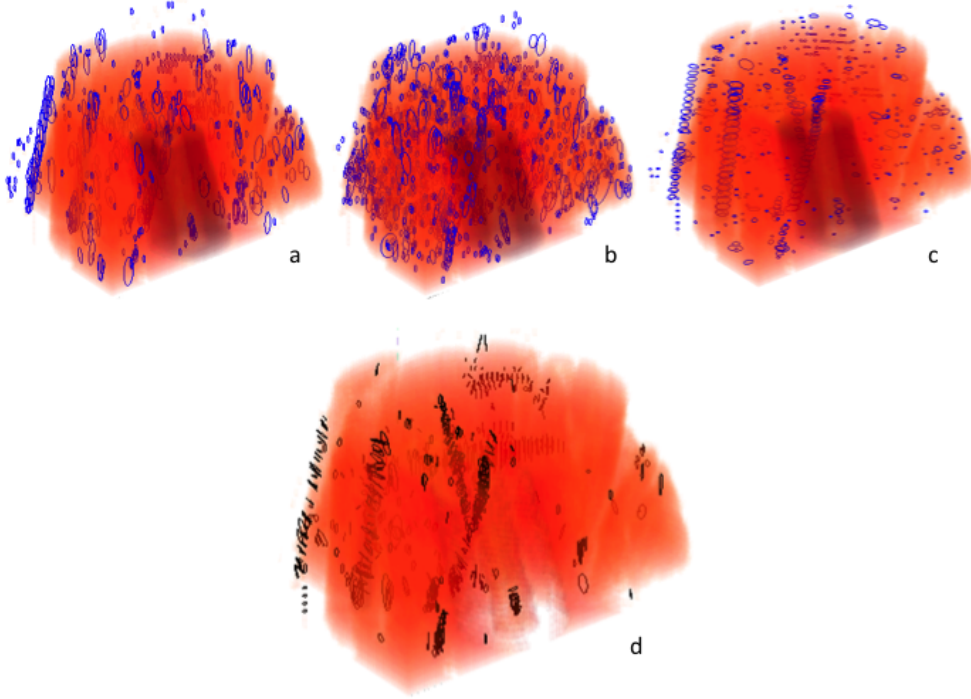


FIGURE 10.2: Shows examples of extracted cross sections. a) Shows cross sections in the coronal plane. b) Shows cross sections in the sagittal plane. c) Shows cross sections in the transversal plane. d) Shows the final cross sections based on the estimated medial line of a vessel. All images shows a 3D profile based on CTA data.

10.2 Define Vessel Segments

In this section the extraction of the extended vessel segments will be described as step two. The purpose of this step is to construct vessel segments by connecting the cross sections B_j from step one, which is described in previous section. The result is a set of segments $\mathbf{S} = \{S_k, k = 1, 2, \dots, N_S\}$ where each S_k is represented by a sequence of $B_k \in \mathbf{B}$. The segments are derived from a graph represented with B_j as vertices and edges as two connected cross sections.

To establish a valid connection between two cross sections: B_{j1} and B_{j2} they must satisfy the conditions in equation 10.11, 10.12, 10.13 and 10.14.

$$\|c_{j1} - c_{j2}\| \leq 3 \text{ voxels} \quad (10.11)$$

$$\arccos(|n_{j1} \cdot n_{j2}|) \leq 50^\circ \quad (10.12)$$

$$\begin{aligned} \arccos(|n_{j1} \cdot \frac{(c_{j1}-c_{j2})}{\|c_{j1}-c_{j2}\|}|) &\leq 50^\circ \\ \arccos(|n_{j2} \cdot \frac{(c_{j1}-c_{j2})}{\|c_{j1}-c_{j2}\|}|) &\leq 50^\circ \end{aligned} \quad (10.13)$$

$$c_{j1} \text{ and } c_{j2} \text{ can be linked with a constraint region growing method} \quad (10.14)$$

The conditions 10.11, 10.12, 10.13 setup conditions on the similarity between B_{j1} and B_{j2} . First condition secure distances between the cross sections remain close for a vessel structure. In this work a 3 voxel distance is selected as the maximum distance to create a valid connections. Note that the data is anisotropic, thus the spatial distance is larger in the transversal plane. The second condition limits the curvature between B_{j1} and B_{j2} . The third condition in equation 10.13 requires the connection line between c_{j1} and c_{j2} and the cross sections to be kept relatively perpendicular measured on the cross sections normal.

If B_{j1} and B_{j2} pass the three described conditions the connection analysis continue to the last condition, which requires the cross sections can be connected with a region growing method. The test is setup in two steps. First a smooth surface is constructed between B_{j1} and B_{j2} to simulate a vessel tube connection. Secondly a adaptive region growing is initialised with c_{j1} as seed point, and continue until c_{j2} is included in the vessel volume or the region growing break through the surface, which defines a leakage.

Surface Connection

To model a tubular structure the candidates is considered in pairs with a smooth interpolated surface as boundary. Figure 10.3 illustrates the surfaces between two cross section candidates, which assume non parallel cross sections. Each pair of cross section there are able to fulfil the condition in equation 10.11, 10.12 and 10.13 are transformed into cylindrical coordinates. In the cylindrical domain the ellipsis undergo a sweeping towards each other to create a morphing interpolated surface. Finally the surface is transformed back to Cartesian coordinates.

A more comprehensive description of the surface interpolation is published by Graham [2008].

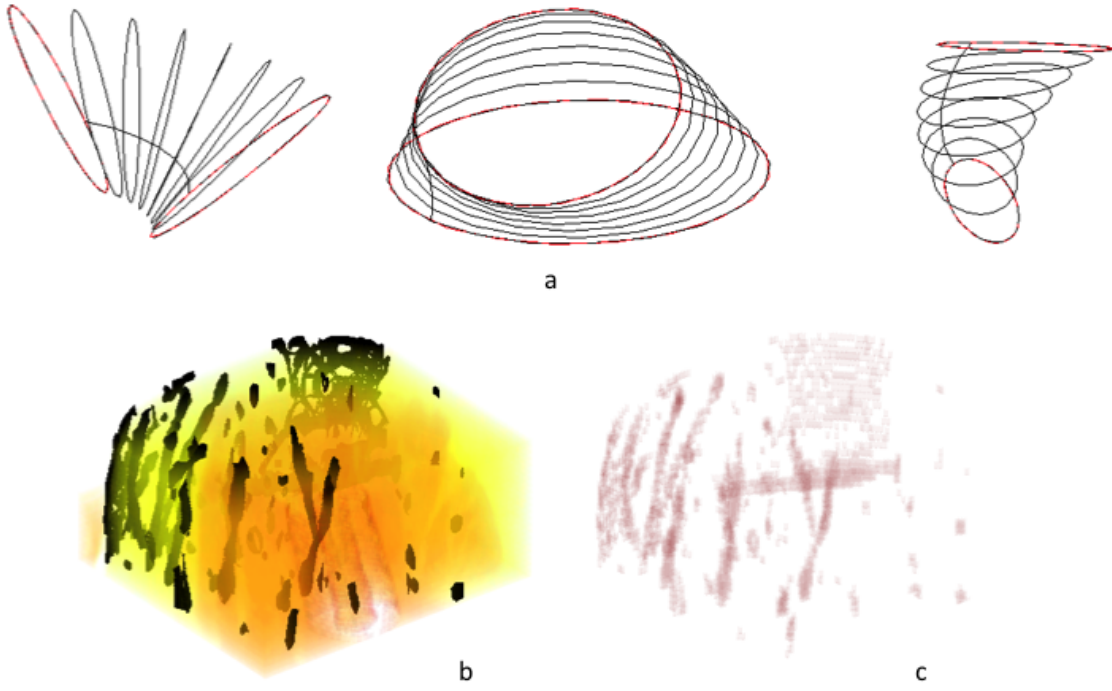


FIGURE 10.3: Illustrates different method concepts in the definition of vessel segments. a) Shows three illustrations of the interpolation between two cross sections. b) Shows the interpolated surface superimposed on CTA data. c) Shows the defined vessel segments as voxel volumes.

The interpolated surface constitute a volume denoted $R_{j1,j2}$ with B_{j1} and B_{j2} as the end caps. The region grow method is adaptive according to the intensities in $R_{j1,j2}$, and includes voxels with intensities above an intensity threshold. The threshold is initialised to the intensity in c_{j1} and use a 6-connectivity to investigate neighbour voxels.

The intensity threshold is iteratively decreased with ten until c_{j2} is included in $R_{j1,j2}$ or leakage occur. A linkage of c_{j1} and c_{j2} with at least one threshold and without leakage let B_{j1} and B_{j2} pass the last connection condition.

Each valid $\{B_{j1}, B_{j2}\}$ pair in the graph \mathfrak{R} are assigned a set of threshold $\tau(\{B_{j1}, B_{j2}\})$ which link c_{j1} and c_{j2} without region growing leakage. In addition the local segment volume is measured with a score calculated with equation 10.15.

$$f_{j1,j2} = \max_{t \in \tau(\{B_{j1}, B_{j2}\})} f(R_{j1,j2}^t) \quad (10.15)$$

$$f(R_{j1,j2}^t) = -\max_{(x,y,z) \in \partial R_{j1,j2}^t} \{I(x,y,z)\} + \frac{1}{|R_{j1,j2}^t|} \sum_{(x,y,z) \in R_{j1,j2}^t} I(x,y,z)$$

A segment S_k consist of a sequence of $\{B_{1j}, B_{1j}, \dots, B_{1M}\}$ where $M \geq 2$ and the segmented vessel lumen is defined in equation 10.16.

$$R_k = \bigcup_{m=1}^{M-1} R_{jm,jm+1} \quad (10.16)$$

For each segment the following properties must be fulfilled:

1. $B_{jm} \in \mathbf{B}$ for all $m=1,2,\dots,M$.
2. A consecutive pair $\{B_{j1}, B_{j2}\}$ for $m=1,2,\dots,M-1$ creates an edge in \mathfrak{R} .

3. $\bigcap_{m=1}^{M-1} \tau(\{B_{j1}, B_{j2}\}) \neq \emptyset$ and requires one threshold that can establish all edge for a segment.

Finally the S_k is assigned a score calculated with equation 10.17. In this work a B_j is assigned to the segment which obtain the highest $S_{score,k}$ score. To find these segments a undirected acyclic graph is constructed for each threshold, where from all linked cross sections is extracted as a segments. Next the segments is sorted based on $S_{score,k}$ wherefrom the highest scoring segments can be determined. If a segment shares a cross section with a higher scoring segment this segment is discarded.

$$S_{score,k} = \sum_{m=1}^{M-1} f_{jm.jm+1} \quad (10.17)$$

10.3 Extended Vs. Original Method

In this section an overview is presented to state the difference between the original method by Graham et al. [2010] and the extended method in this application. In table 10.1 an overview of the differences are presented. In the original method a linear interpolation method is used to produce a isotropic data set. In this application this step was omitted to reduce processing time. However, Graham et al. [2010] claims that isotropic data provides an optimised elliptic fit compared to anisotropic data.

The difference in intensity range is based on the difference in target structure. In this application the intensities was adapted to a brighter appearance due to contrast etc. The intensity iteration step was used in both the 2D cross section filtering scan and the region growing constrained by the interpolated surface. In this application an intensity iteration step on ten was selected to reduce processing time. As applied in the original method an iteration step on 1 would be preferred due to a better elliptic fit in the 2D cross section scan and more accurate region growing.

In the original method a max threshold was used to limit the number of 2D cross sections and segments. In this work such thresholds was not considered applicable due to differences among data sets..

A pair of cross sections must fulfilled the conditions presented in section 10.2 to obtain a valid connection. In this application 50 instead of 60 degrees was used to reduce processing time. The selection of 3 voxel instead of 3 mm was required due to anisotropic data.

In the original method a no backtracking condition was made to constrain the sequence of cross section in a segment. In this application the backtracking condition was not applied, since larger segments was preferred.

<i>Issue</i>	<i>Extended Method</i>	<i>Original Method</i>
Isotropic data	no	yes
Intensity range	1100-1500	0-600
Intensity Iteration Step	10	1
Max 2D CS count	unlimited	750,000
Max segments	unlimited	1500
CS pair geometry difference	<50°	<60°
Max CS pair distance	3 voxels	3 mm
CS backtracking in segment	yes	no

TABLE 10.1: The table presents the main differences between the original and adapted method for this application. Note that cross section is denoted 'CS'.

Chapter 11

Stage 3: Merge Segmentations

In this chapter the last segmentation stage is described. The purpose of this stage is to generate the final segmentation based on the initial segmented vessel tree from stage 1 and extracted segments from the extended method in stage 2.

11.1 The Merging of Extracted Volumes

In this section the approach to merge and extract the final volume is described. The extended segmentation method from stage 2 provides a large amount of segments that apparently represents vessels. However, since the steps in stage two consider a broad range of intensities segments from stage 2 contains both true positive and false positive vessel segments.

In this final stage the segments is connected to the initial vessel tree by using a similar region growing method to the region growing method in stage 1. The approach is to use the voxels in the extracted segments as seed points. From each segments separately, the region growing method is initialised. If the included voxel volume intersects with another segment or vessel tree the connection voxels is accepted. However, the amount of voxel volume is constrained with a maximum voxel count empirical set to 50 voxels in this application.

The merging of vessel tree and segment concept is illustrated in figure 11.1. The dashed shapes represents the connection voxel volume extracted with region growing. In case '1' the segment is unable to connect to any segments or the vessel tree. In case '2' the segment is connected to the vessel tree. However, the segment also progress in the opposite direction of the vessel tree, which either extend segment with vessel dedicated voxels or progress into non vessel structures. In case '3' the segment is nicely connected to the vessel tree and produce a successful vessel extension to the initial extracted vessel tree. Case '4' shows a successful connection between two segments. The final vessel volume is extracted by including all voxels in a 26-connected neighbourhood initialised with the manual seed point from stage 1.

The Merging Algorithm

An overview of the stage 3 algorithm is presented as pseudo code in algorithm 2. There are two empirical selected parameters. The first parameter is the minimum voxel size of segment (MSS). The second parameter is the maximum connection volume.

In this application MSS is selected to 10 voxel and the maximum connection volume is set to 50

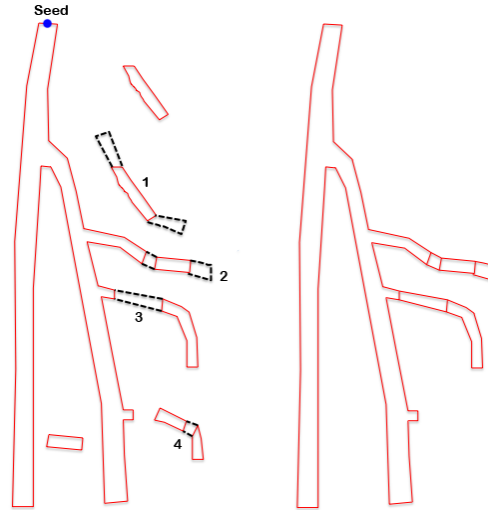


FIGURE 11.1: Shows the concept of connecting segments and the vessel tree. The segments 1-4 represent four cases of segment connections.

voxels. The purpose of the merging algorithm is to extract a full connected vessel tree. After all connections are performed on the segments and initial vessel tree a full connected vessel tree is extracted using a 26-connected neighbourhood initialised from the manual selected seed point.

Algorithm 2 Describes the algorithm to connect segments with the initial extracted vessel tree.

Require: Initialization of parameters

- 1: {Run through segments with voxel count $> \text{MSS}$ }
 - 2: **for** $k=1:\text{segment count}$ **do**
 - 3: Initialise region grow on segment voxels with mean intensity
 - 4: **for** $k=1:50$ voxels **do**
 - 5: Include neighbour voxel where $\text{Min}(|I_{\text{neighbour}} - I_{\text{mean}}|)$ to connection volume
 - 6: **if** connection volume \cap segment or \cap vessel tree **then**
 - 7: Accept connection and add connection volume to extracted volumes
 - 8: **end if**
 - 9: **end for**
 - 10: **end for**
 - 11: Find final volume voxels with 26 - connected neighbourhood
 - 12: **return** Final volume
-

Comments on The Stage 3 Concept

The merging algorithm provides a simple region growing algorithm to connect segments and vessel tree. However, the approach inherits the disadvantage of region growing. For instance, suppose a non vessel segment located close nearby a true vessel segment or vessel tree is initialised as seed point. If 50 voxels are sufficient to establish a connection the non vessel segment is accepted. In addition the region growing has no growing direction constraint. Theoretically this may add a extra layer to a segment before the connection is established to another segment or the vessel tree. The approach fits the purpose of connecting segments with a initial vessel, which is the main

priority in this work. Thereby, this work has applied the stage 3 merging method as a delimitation solution instead of the methods in stage 4 and 5 from the original method by Graham et al. [2010].

11.2 Implementation

The segmentation algorithm is developed and implemented in Matlab by Mathworks, version R2011a 64-bit on a Macintosh. Matlab provides a prototype environment, with a variety of embedded algorithm used in the implementation. The implemented algorithm is a prototype where processing time and optimization has been prioritized secondly to the proof of concept. Thus optimisation of the processing time has not been a main priority.

Part IV

Test

Chapter 12

Test

In this chapter the test of the segmentation method is described. In the first two sections the test of the initial and extended segmentation method are presented. In the last section the test results of the complete segmentation is presented and shows the segmented volumes in profiles.

12.1 The Initial Segmentation

In this section the test of the initial segmentation is described. One of the requirements to the initial segmentation is to avoid over segmentation, which is defined as the inclusion of a none vessel volume in the segmented volume. The first test in this section presents the test of the automatic threshold selection. In this test the automatic threshold selection is compared to a manually optimised threshold, now referred to as the 'optimal' threshold, to investigate if the automatic threshold produce over segmentation.

In the second section a test of the extracted volume with the automatic threshold is presented. In this test the difference in segmented volumes with the automatic threshold and the optimal threshold will be evaluated. It is an advantage to extract as large volume as possible in the initial segmentation. Therefore the test investigate the segmented volume to evaluate the effect of using the automatic threshold compared to the optimal threshold.

In the last section the test of the bone filter will be presented. The bone filter is depended on the volume extracted with the initial segmentation. An optimised vessel volume extraction will improve the bone filter to remove less vessel volume. In this test the difference in bone filter is evaluated when the bone filter use the volume from the initial segmentation extracted with different thresholds. In the test the initial segmentation use the automatic and optimal threshold in the comparison.

12.1.1 Selection of Threshold

The initial segmentation stage requires a threshold value to determine the inclusion criteria of a voxel. The purpose of this test is to investigate the automatic threshold selection and compare the results with the optimal threshold.

As described in the method description in section 9 the automatic threshold is determined in two steps. First step initialise the threshold to zero and begin iteratively to increase the threshold. For each threshold the total voxel count in the segmented volume is investigated. When the total voxel

count exceeds 50000 voxels the threshold iterations stops. The second step reduces the threshold value with a conservative factor parameter. In this test the factor parameter is set to 0.5. The reached threshold in step one is multiplied with the factor parameter and rounded to the nearest integer, which is selected as the final threshold(See equation 9.3).

The optimal threshold is selected as the highest reachable threshold before over segmentation occurs. To guide the selection of an optimal threshold a voxel- threshold diagram is used to investigate the curve of voxel inclusion (see figure 12.1). The breaking points, where the voxel inclusion accelerates, are used as guidance to select the thresholds. To evaluate over segmentation the transversal planes in the CTA data are visually evaluated by a none expert.

The thresholds and voxel counts is presented as results in table 12.1.

<i>Data set</i>	Automatic		Optimal		Difference
	<i>Threshold</i>	<i>Voxel Count</i>	<i>Threshold</i>	<i>Voxel Count</i>	<i>Voxels</i>
1	27	8497	49	21225	12728
2	29	12107	57	15755	3648
3	76	4137	151	8998	4861
4	37	13489	67	23508	10019
5	20	13814	25	15959	2145
6	48	8223	69	9989	1766
7	31	11292	40	13823	2531
8	42	23978	54	27041	3063
9	34	14355	50	23211	8856
10	30	10657	45	14258	3601
11	39	22372	40	22560	188
12	35	11497	38	12392	895
13	56	7628	95	9967	2339
14	29	5802	37	6758	956
Mean	38.1	11989.4	58.4	16103.1	4114
Max	76	23978	151	27041	12728
Min	20	4137	25	6758	188

TABLE 12.1: Shows the results from the automatic selection of thresholds and the optimal threshold.

The voxel counts varies from 6758 to 27041 voxels with the optimal threshold and 4137 to 23978 voxels with the automatic threshold. Since the optimal threshold produce the largest volume without over segmentation the automatic threshold must ensure not to exceed the optimal threshold. As shown in table 12.1 this requirement is fulfilled for each of the data set.

To illustrate the voxel inclusion pattern figure 12.1 shows a graph with seven curves based on data set 8 to 14. The graph illustrates the different patterns in the voxel inclusion among the data sets. This stresses the requirement of a conservative selecting threshold approach to fit all data set.

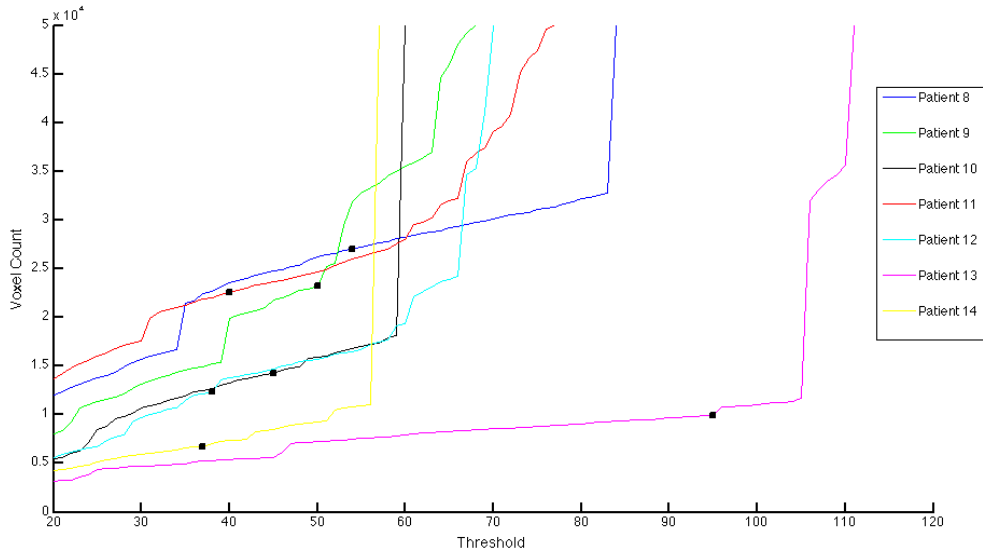


FIGURE 12.1: Shows a voxel- threshold diagram with seven curves representing data set 8 to 14. The black markers represent the optimal threshold for each of the data set.

12.1.2 The Initial Vessel Tree

The purpose of this test is to investigate the amount of segmented vessel volume and compare the volumes extracted with the automatic threshold and the optimal threshold.

As described in previous section the optimal threshold produce no over segmentation, and ideally the automatic selected threshold should approach the optimal threshold to extract the maximal possible volume without over segmentation. However, as presented in table 12.1 none of the automatic threshold is equal to the optimal threshold. The volume differences range from 188 voxels in data set 11 to 12728 voxels in data set 1. To illustrate the difference in extracted volumes, the extracted vessel from data set 1 and 11 are shown in Figure 12.2.

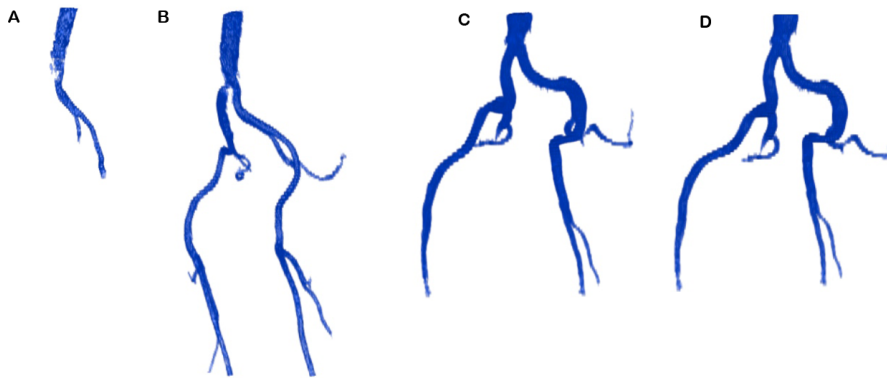


FIGURE 12.2: Shows four extracted vessel trees with the initial segmentation. A) Shows the vessel tree extracted with the automatic threshold from data set 1. B) Shows the vessel tree extracted with the optimal threshold from data set 1. C) Shows the vessel tree extracted with the automatic threshold from data set 11. D) Shows the vessel tree extracted with the optimal threshold from data set 11.

In this test the majority of the vessel trees contains the common-, internal- and external iliac.

However, the depth and number of branches varies among the data sets. Note that all initial segmented vessel volume profiles are illustrated in section 12.3.

12.1.3 Bone Filtering

The purpose of this test is to investigate the effect of the bone filter on the big vessels. Since the initial segmentation is used to adjust the bone filter (See equation 9.4 in section 9) the removal effect may be different when the automatic or optimal vessel tree volume is used as filter adjustment. Therefore the purpose of this test is also to test the difference between the two bone filter volumes. As described in the method description in Section 9 the filter use a binary image to detect bone structure. The filter design uses a spatial threshold on 200 voxels and an intensity threshold on 1200. The low intensity threshold is in the vessel intensity spectrum and therefore enables removal of the bigger vessel unless the initial segmentation is able to make sufficient filter adjustment. In table 12.2 the results of the filter volume are presented. Ideally the automatic threshold and optimal threshold in the initial segmentation should approach an equal filter volumes.

As shown in the table the difference in bone filter volume is zero and thereby equal in data set 2 and 5. Six data sets have a volume difference fewer than 50 voxels while data set 9 has a volume difference on 1450 voxels.

<i>Data Set</i>	<i>Automatic Voxel count</i>	<i>Optimal Voxel count</i>	<i>Difference Voxels</i>
1	232428	231913	515
2	438690	438690	0
3	111218	111206	12
4	559803	559409	394
5	446799	446799	0
6	305537	305534	3
7	551206	550724	482
8	405070	404087	983
9	425250	423800	1450
10	381621	381469	152
11	467922	467903	19
12	348448	348090	358
13	270836	270815	21
14	299187	299082	105

TABLE 12.2: Shows the results from the bone filter test. For each data set the bone filter effect is measured with a voxel count adjusted with the automatic and optimal threshold in the initial segmentation. The delta count is the difference in voxel count between the two filters.

In figure 12.3 the two bone filters in data 9 are illustrated in two transversal planes. The figure shows a yellow label to represent the shared bone filter volume and red label to represent the bone filter adjusted with the automatic initial vessel tree. The latter bone filter shows more coverage of bigger vessel, thus in this case the filter remove more vessel volume when the filter adjustment is performed with the automatic extracted vessel tree compared to the bone filter adjusted with the optimal vessel tree.

The test results show the bone filter is depended on the quality of the initial segmented vessel tree. The demonstrated case in figure 12.3 shows the downfall of the automatic threshold selection if the extracted vessel tree is insufficient to remove big vessel in the bone filter volume.

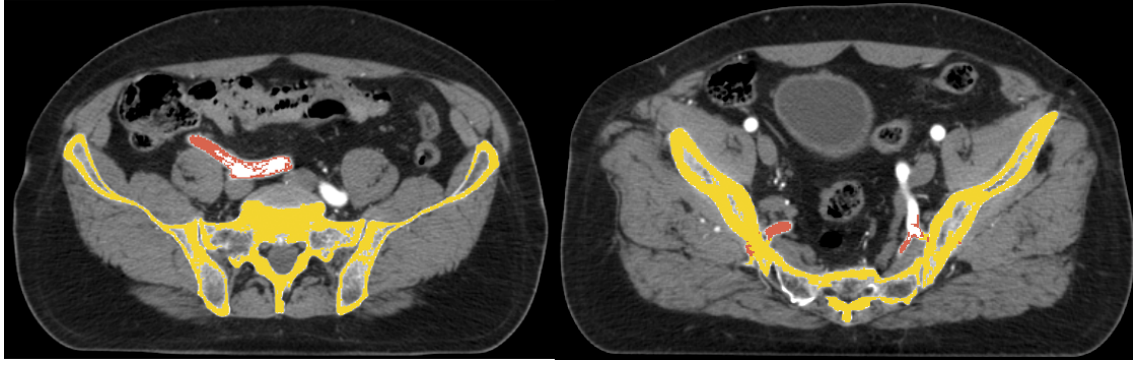


FIGURE 12.3: Shows two transversal slice in data 9. The yellow labels represent the shared volume between the two bone filters bone filter. The red colour label represents the bone filter adjusted with the automatic initial vessel tree.

12.2 The Extended Segmentation

In this section tests of selected topics within the extended segmentation method are described. First the amount of connected segments is tested. Secondly there will be a test of the overall segmentation performance.

12.2.1 Extracted Segments

The purpose of this test is to evaluate the number of extracted segments and the number connected segments in the final vessel tree.

As described in the method description(See section 11.1) the merging of the initial vessel tree and extracted segments (In the third segmentation stage) use two parameters. The first parameter is used to remove extracted segments with small volumes and is a simple threshold that defines a minimum segment volume. In this test ten voxels is used as the minimum segment volume.

The second parameter is used to define the maximum needed volume to connect segments and the vessel tree. A connection between segments and the initial vessel tree is established with region growing using each segment voxels as seed voxels. A connection is established when the region growing includes a intersecting voxel with another segment or vessel tree. However, a connection is only valid if the intersection can be established within a maximum voxel threshold on fifty voxels.

The results are presented in Table 12.3 and shows: The total number of segments produced by stage two segmentation, the number of segments above ten voxels and the number of segments in the final volume.

In data set 1 the highest number of segments is extracted with a number on 9314 segments and is above nine times the amount of data set 14. Data set 3 connects the highest number of segments to the final tree volume. With both the automatic and optimal initial vessel tree, using a minimum voxel criteria above 10 voxels reduces tree the number of segments. In most of the data sets the segment counts are reduced to one fourth of the total segment count.

Data Set	Total	Automatic		Total	Optimal		Difference Connected
		>10	Connected		>10	Connected	
1	9314	1459	89	9393	1472	137	48
2	1357	304	58	1362	303	62	4
3	1668	444	133	1667	445	151	18
4	2727	474	66	2714	474	75	9
5	1621	367	24	1629	364	25	1
6	1415	374	31	1417	375	31	0
7	2277	409	22	2278	410	38	16
8	1478	329	32	1469	322	34	2
9	1189	246	18	1200	246	37	19
10	1446	264	13	1452	264	18	5
11	1694	395	23	1702	397	23	0
12	1902	379	32	1899	378	35	3
13	2084	443	51	2072	433	45	6
14	634	152	19	778	164	14	5
Mean~	2200	431	44	2217	432	52	10
Max	9314	1459	133	9393	1472	151	48
Min	634	152	13	778	164	14	0

TABLE 12.3: Presents the number of segments extracted with the extended method.

To illustrates some of the extracted volume Figure 12.4 shows a transversal slice labelled with all segments related to this slice. The labelled image shows that both vessel and bone structure is extracted. However the extracted method is able to extract smaller structure in areas of more branches. In this figure the branches is connected to the internal iliac.

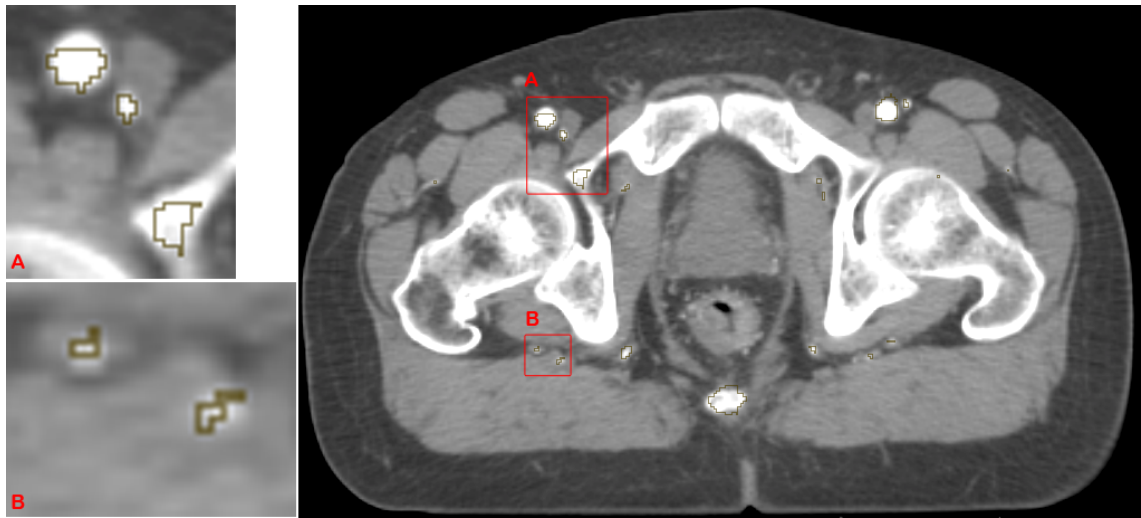


FIGURE 12.4: Shows a CTA image in the transversal plane with labelled extracted volumes. A) Shows that the external iliac and a smaller vessel are detected. However, in addition a bone structure is extracted as a segment. B) Shows a small vessel originated from the internal iliac, which may be disconnected duo to the bone filter. The Figure is based on data set 6

To illustrate an extracted segment volume figure 12.5 shows the difference between the extracted segment volume and the final vessel tree from one data set. The segment pool contains false positives, which is marked in the region 'A' in the figure. However region 'B' also shows a potential extension of the vessel tree that may connect more vessel branches.

The test results shows that the extended segmentation extract a pool of segments with vessel volumes and non vessel volumes. The vessel volumes provide a potential further vessel branch segmentation. However, the connected segments must be distinguished from non vessel segments.

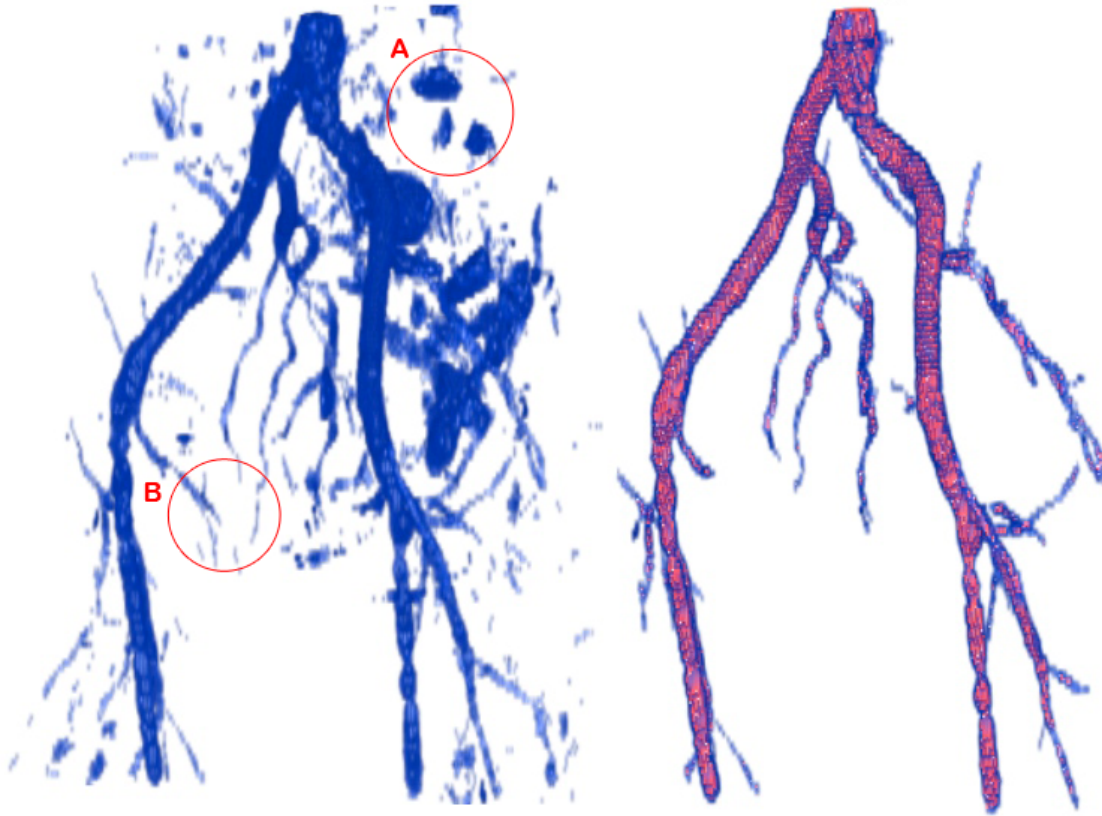


FIGURE 12.5: Shows the volume profiles representing from left two right the extracted segments and the final vessel tree with automatic initial threshold. Region 'A' illustrates a volume containing false positive segments. Region 'B' shows some potential vessel extension to the final vessel tree.

12.2.2 Performance of Segmentation

The purpose of this test is to investigate the performance of the entire segmentation method.

Figure 12.6 illustrates a labelled segmented volume in two CTA slices in the transversal plane. The blue contour represents a segmented volume based on the extended vessel segmentation and the brown contour shows the initial segmentation vessel tree. In the zoomed region 'A' the blue contour shows a volume extracted with the extended method. Region 'B' and 'C' shows a blue contour with a brown inner contour representing the initial segmentation. Based on a visual evaluation the region 'A' shows, that the extended segmentation is able to extract vessel structures with no connection to the initial tree, however in the red circle the blue contour includes a small volume with a dark appearance, which is considered a false positive vessel structure. A similar case is illustrated in region 'B' and 'C' where the blue contour applies an extra layer to the initial segmentation and produce over segmentation. In contrary the brown contour shows a well segmented vessel structure. In general the extended method produce over segmentation in each of the data set. The segments from the extended segmentation lack of a reasonable fit to the vessel walls and thereby apply an extra over segmented layer to the initial segmentation. However the initial segmentation is able to extract vessel volumes without over segmentation by using an automatic detected threshold in the initial segmentation method.

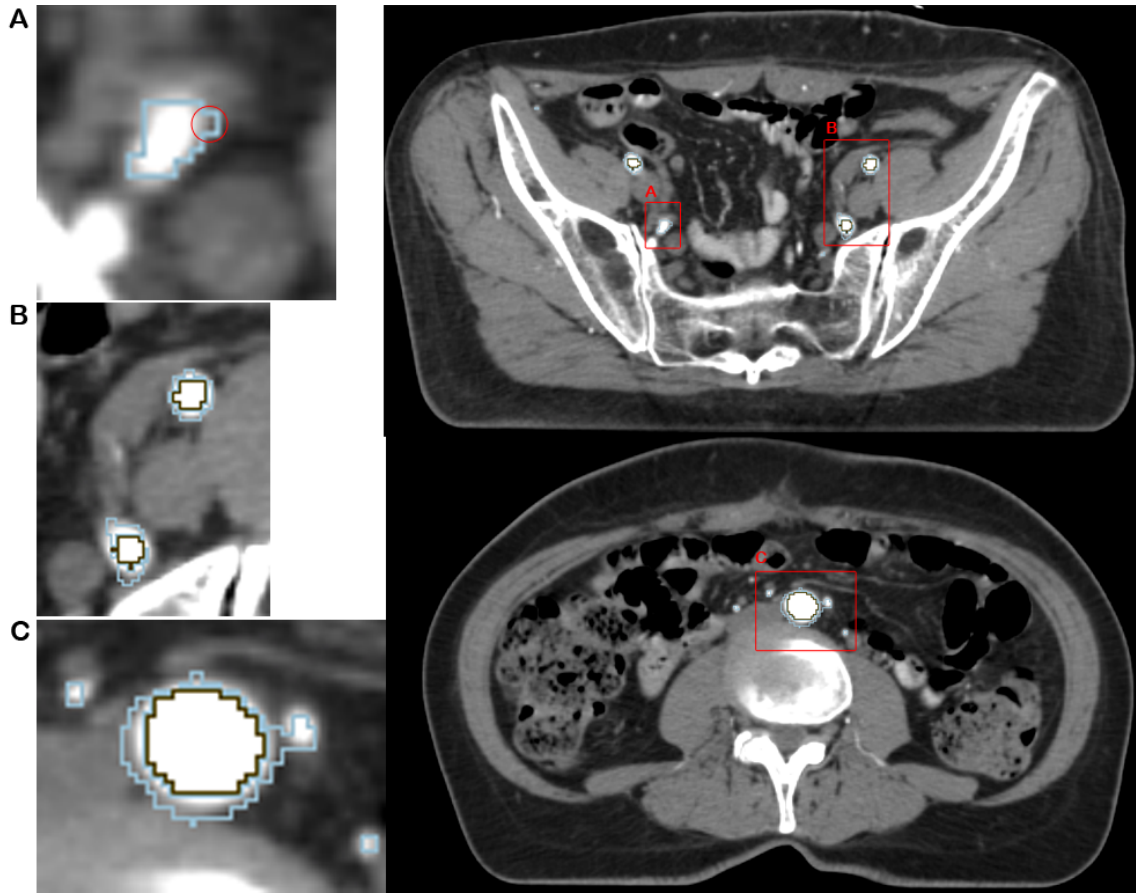


FIGURE 12.6: Shows a CTA image in the transversal plane with labels representing the extracted volumes. The brown contour represents the volume extracted with the initial segmentation. The blue contour is the volume extracted with the extended method. Region 'A' shows a segmented vessel with the extended method. Region 'B' and 'C' shows contours where the extended method to adds an extra layer to the extracted volume. The figure is based data set 6.

12.3 Segmentation Profiles

In this section all the segmented vessel volume profiles are presented. Figure 12.7 to 12.20 shows the segmented volumes from each of the fourteen data sets. The figures contain four segmented vessel volumes. The first two vessel trees from the left are based on the automatic selected thresholds (AST). The last two vessel trees from the left are based on the optimal thresholds (OT). The blue volumes show the initial segmentation in stage one and the red volumes are extracted with the merging segmentation method in the stage three.

In data set 1 (Figure 12.7) the AST initial vessel trees lack of big vessel segmentation. In addition the extended method has no visual vessel branch gain. The OT initial tree produce several big vessels compared to the AST tree however, the extended segmentation does not add considerable vessel branches. In data set 2 (Figure 12.8) the initial vessel tree with AST and OT has a similar segmented profile. The extended method shows a gain of several extra vessel branches.

In data set 3 (Figure 12.9) the OT initial tree contains more vessel branches compared to the AST tree. However, the extended segmentation produce a severe over segmentation in both the AST and OT extended tree.

In data set 4 to 6 the initial tree with both AST and OP produce similar profiles, however with more volume in the OT trees. The extended trees shows more segmented vessel branches compared to the initial trees.

The profiles from data set 7 and 9 the effect of the bone filter are illustrated. When the initial segmented tree volume is insufficient, the bone filter removes big vessels. As shown in both data set 7 and 9 some big vessels (especially right external iliac vessel) are absent compared to the OT vessel trees.

In data set 13(See Figure 12.19) the extended vessel tree are severe over segmented in the top of the vessel tree.

In these tests, data set 11 and 14 have shown the best results in terms of lower over segmentation and segmentation of finer vessel structures (See figure 12.17 and 12.20).

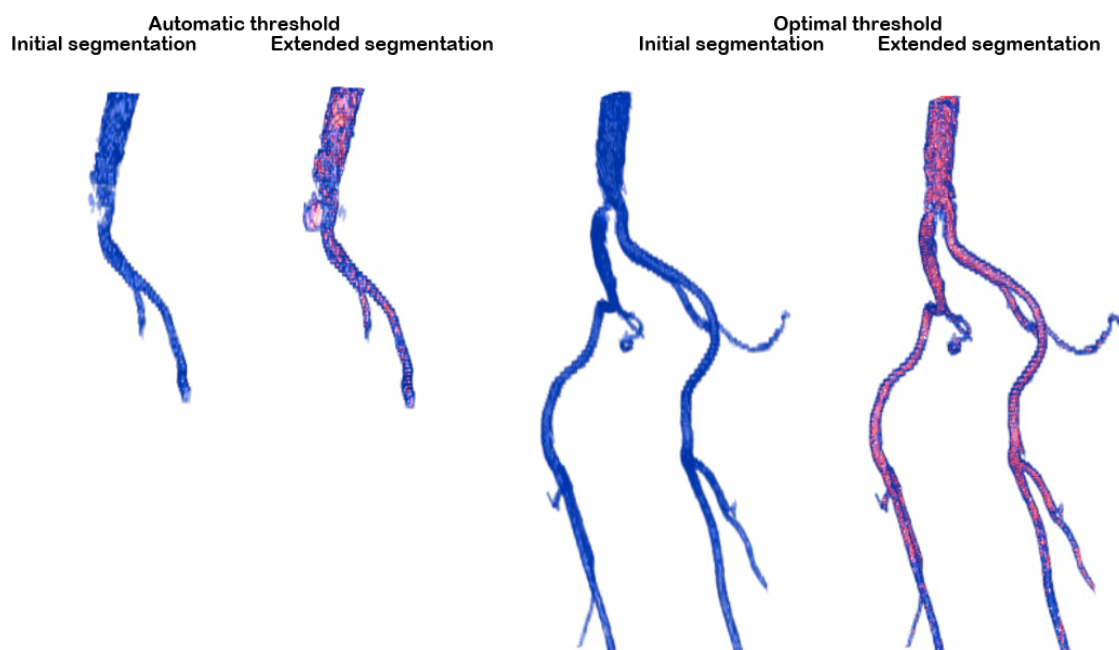


FIGURE 12.7: Shows the segmented volumes is based on data set 1.

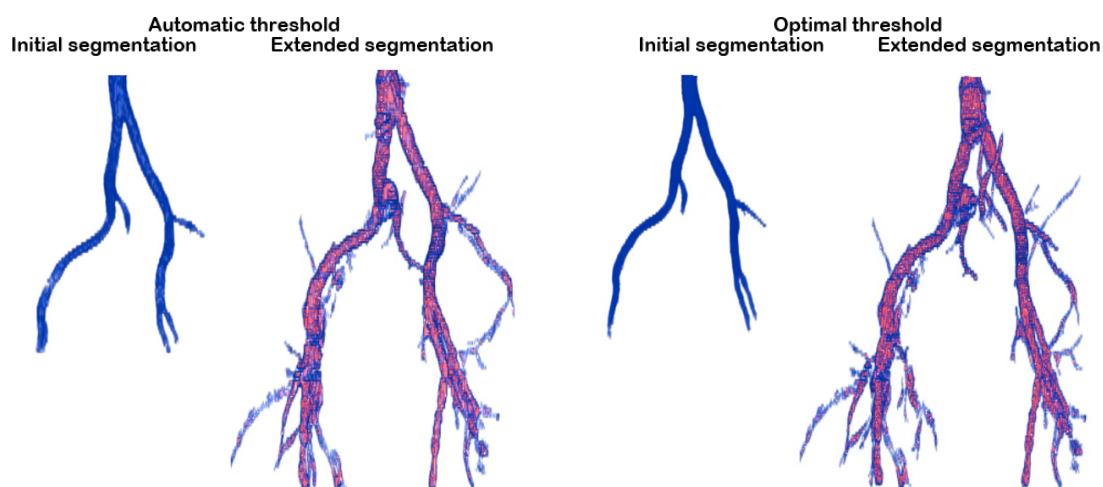
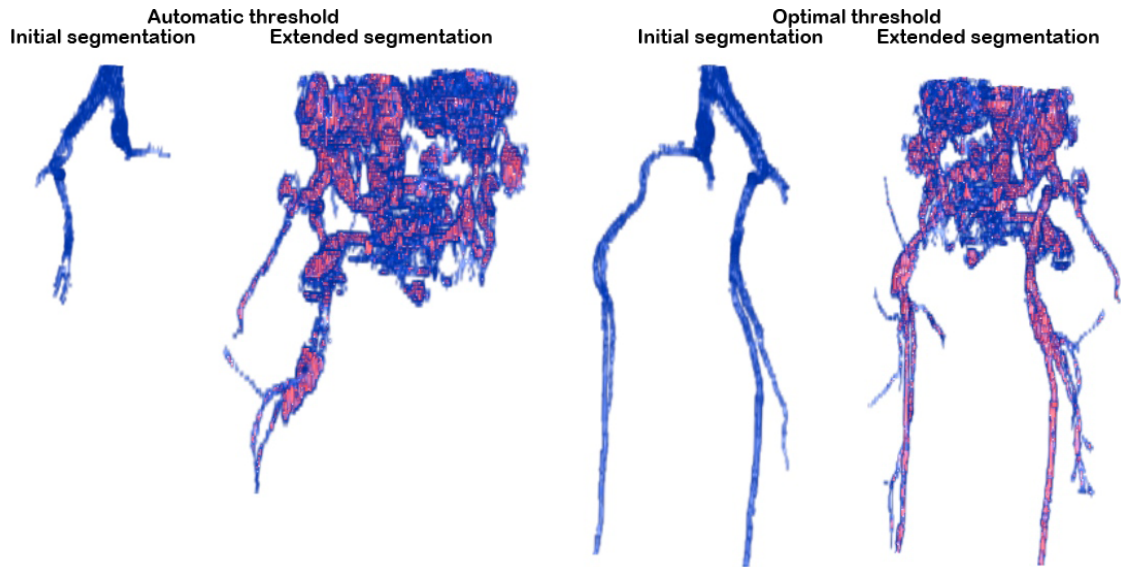
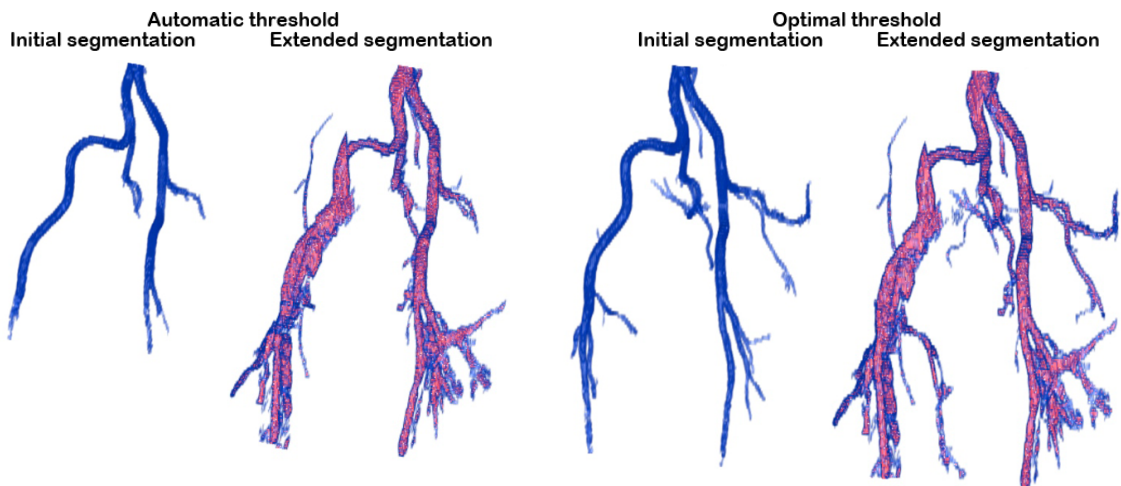


FIGURE 12.8: Shows the segmented volumes in data set 2.

FIGURE 12.9: *Shows the segmented volumes in data set 3.*FIGURE 12.10: *Shows the segmented volumes in data set 4.*

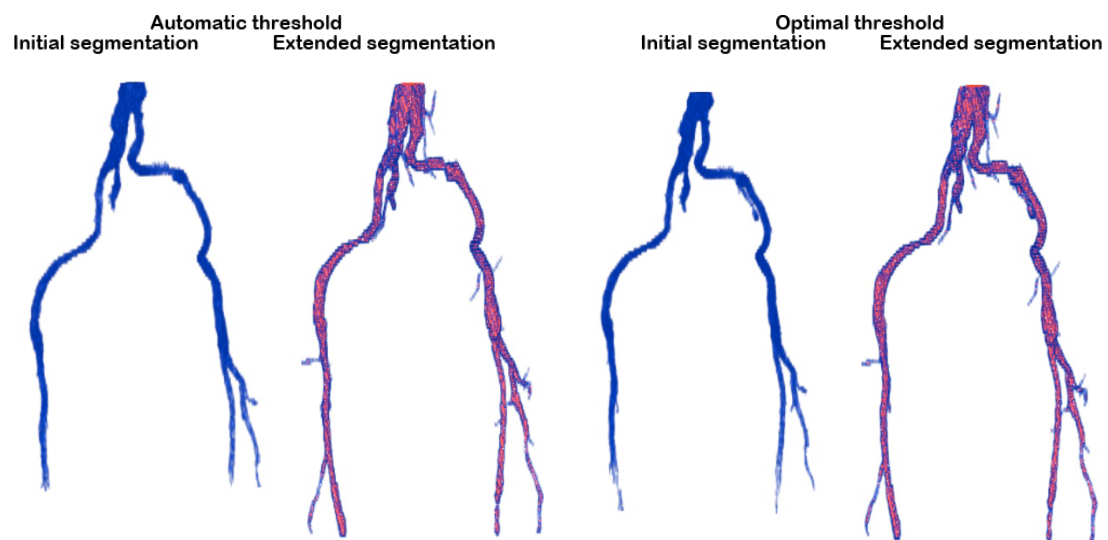


FIGURE 12.11: Shows the segmented volumes in data set 5.

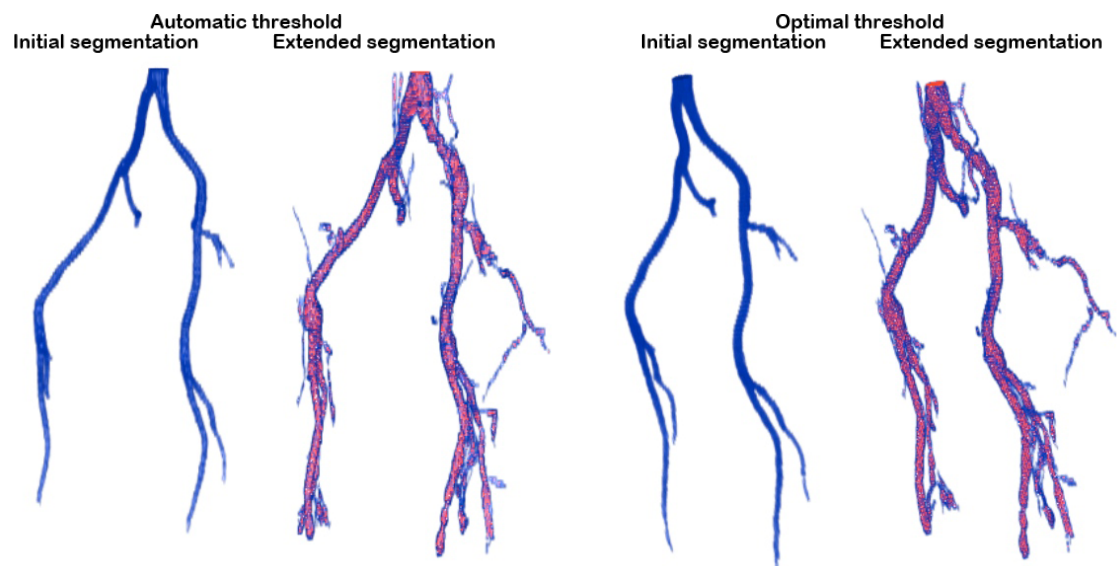


FIGURE 12.12: Shows the segmented volumes in data set 6.

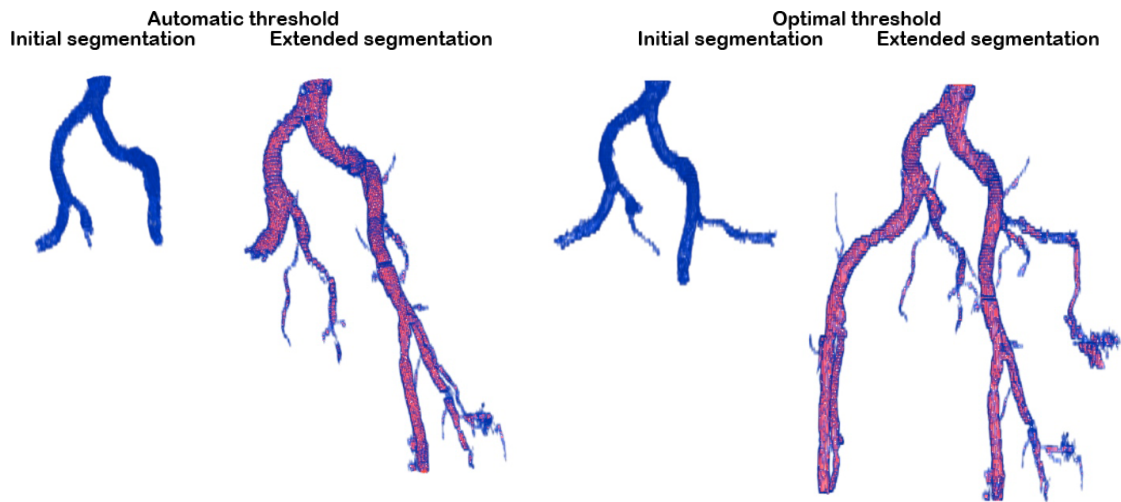


FIGURE 12.13: Shows the segmented volumes in data set 7.

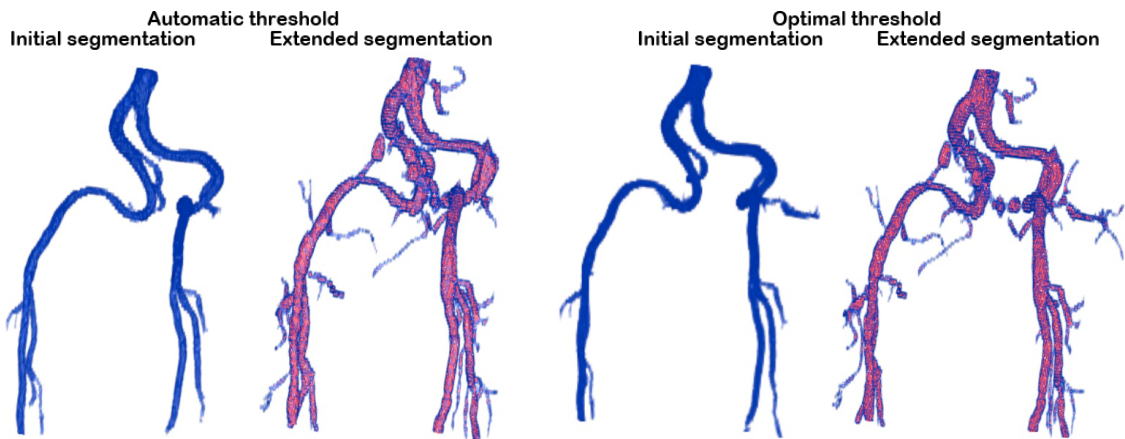


FIGURE 12.14: Shows the segmented volumes in data set 8.

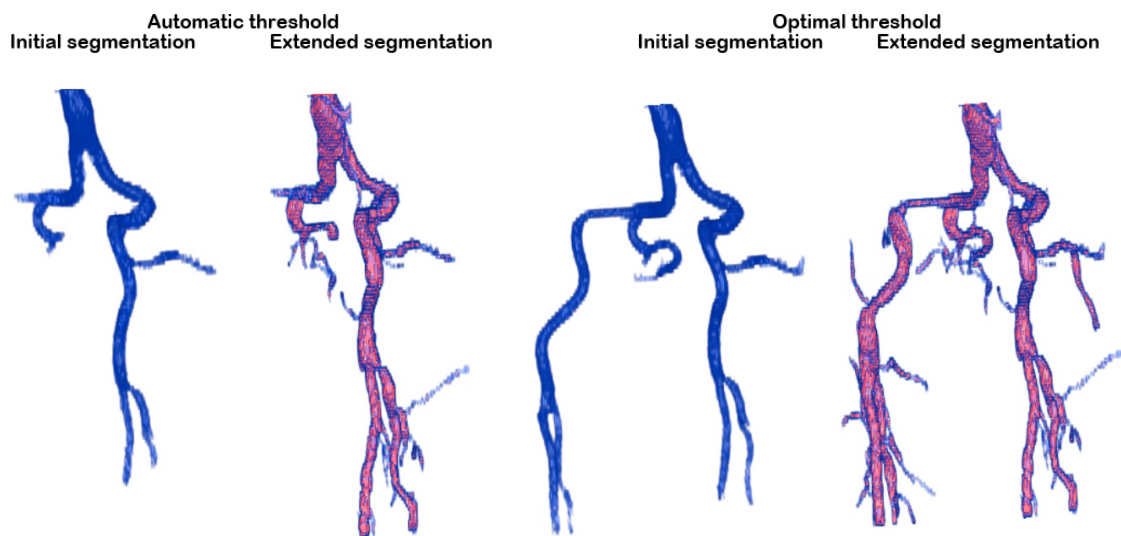


FIGURE 12.15: Shows the segmented volumes in data set 9.

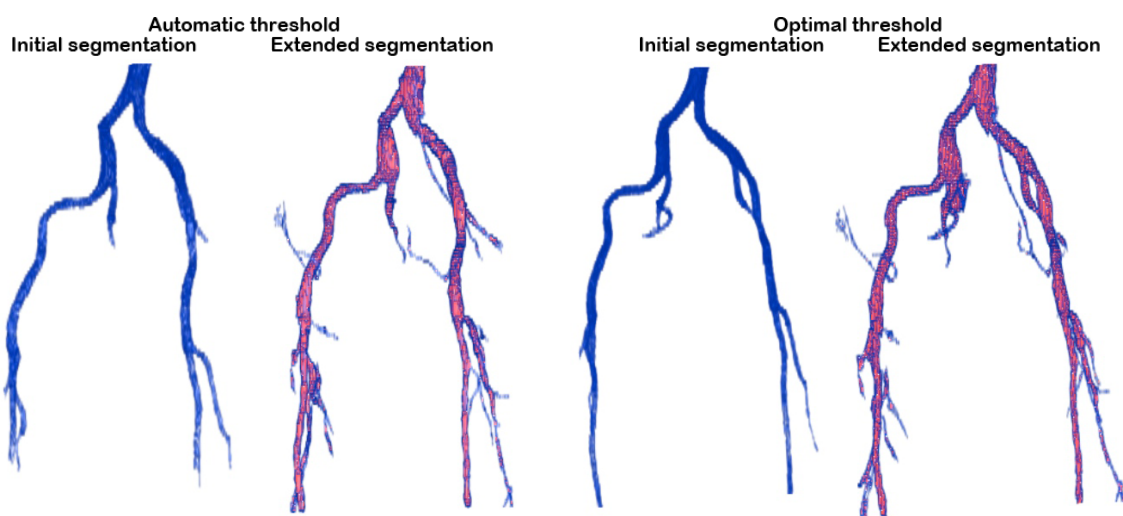


FIGURE 12.16: Shows the segmented volumes in data set 10.

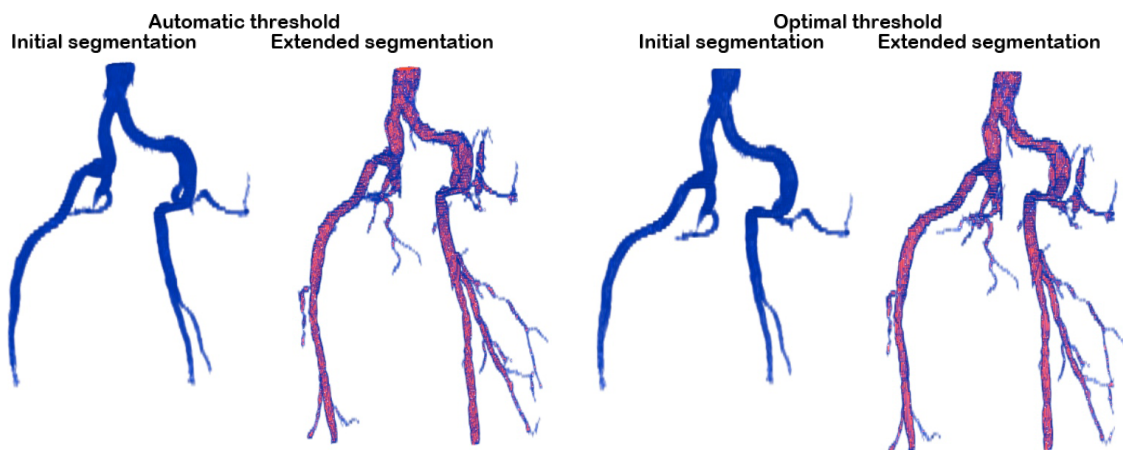


FIGURE 12.17: Shows the segmented volumes in data set 11.

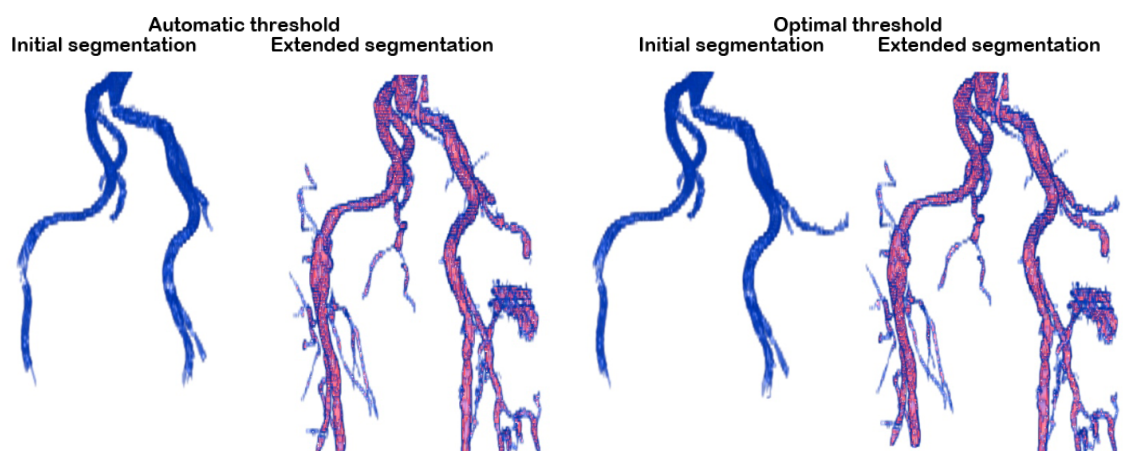


FIGURE 12.18: Shows the segmented volumes in data set 12.

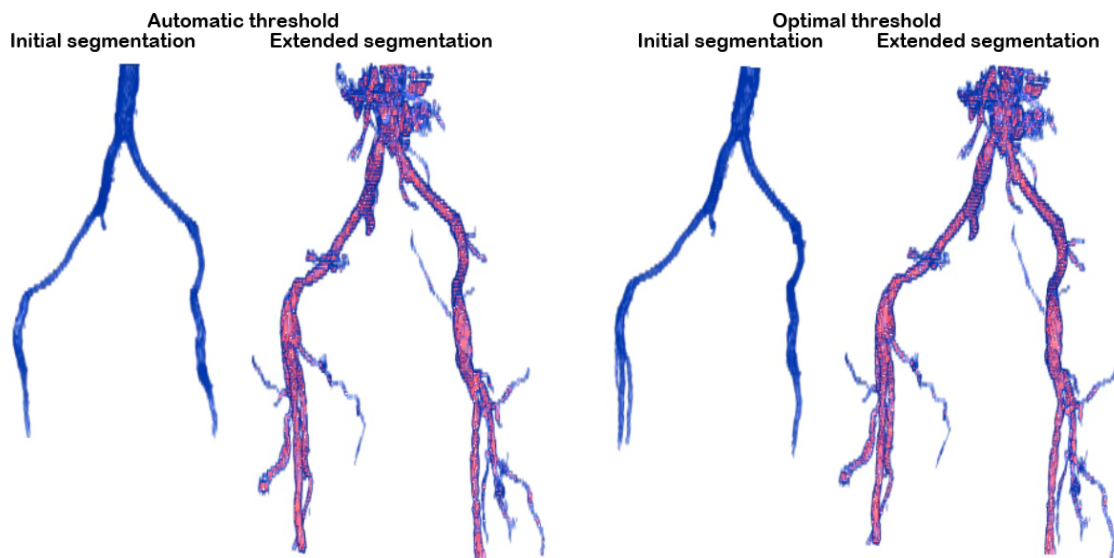


FIGURE 12.19: Shows the segmented volumes in data set 13.

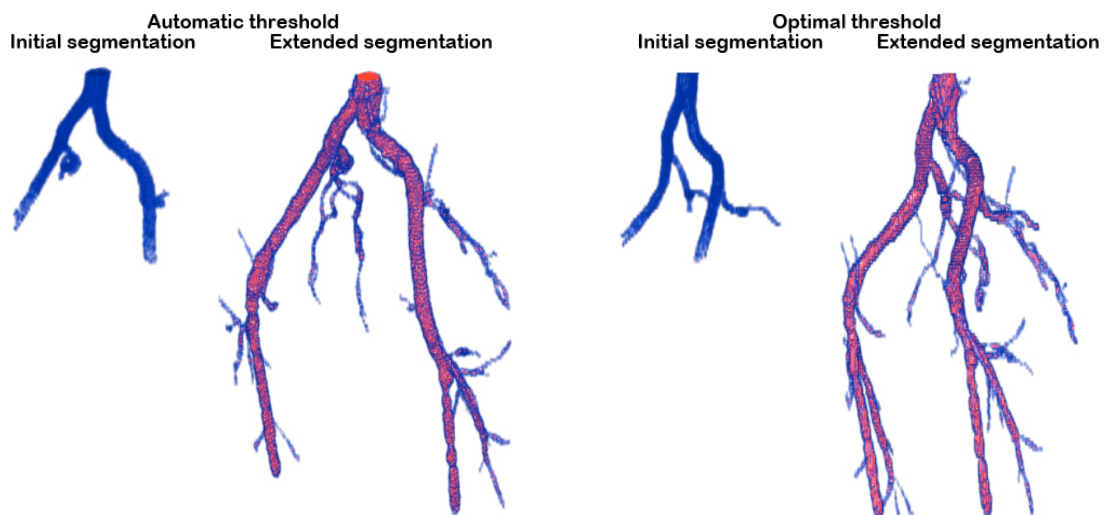


FIGURE 12.20: Shows the segmented volumes in data set 14.

Part V

Recapitulation

Chapter 13

Discussion

13.1 Summary

Cancer has one of the highest mortalities in the world and cancer in the pelvic region is estimated to 27.9 percent of all diagnosed cancers. Today one of the conventional treatments is radiotherapy, which is a selective treatment in terms of targeting cancer cells. However, the outcome of radiotherapy is highly depended on the delineation of cancerous tissue. The clinical target volumes are determined based on medical imaging such as CT and MRI. IGRT and especially IMRT enable a precise irradiation of the clinical target volume and thereby minimise healthy tissue damage.

A common site of spread is the lymph nodes, which are difficult to detect with IGRT images due to poor visual appearance in image modalities. Since the most important lymph nodes are located adjacent to arteries, one approach to improve the detection of lymph nodes is to use enhanced vessel as a surrogate. Several studies have used margins on detected vessels to delineate lymph nodes. However, the arteries are manually detected which is tedious work and time consuming. This has suggested the development of a vessel segmentation method to extract artery volumes and further apply margins to delineate the lymph nodes. In this work the aim was to develop a image segmentation algorithm to extract artery volumes in vessel enhanced images.

The designed method consist of a three stage method and was tested on bolus tracked CTA images captured from patients with rectal and rectum cancer. A main priority in the development was to apply an semi automatic approach with a minimum amount of human interaction. The first stage is a initial segmentation based on a region growing method and need one manual selected seed point. The criteria to include voxel in the segmented volume is a global threshold, which was determined automatically. With the initial segmentation volume, the method apply a bone filter to remove bone structure in the data for later image processing.

The second stage is a extended segmentation and adapts a method, which previously was developed to bronchoscopy. The approach use elliptic 2D cross section features to estimate tube like segments. The final stage in the segmentation method merge the initial segmented vessel volume and the tube like segments from the extended segmentation. This is done with a simple region growing connection scheme.

13.2 Discussion

The Initial Segmentation and Bone Filtering

In the test of the initial segmentation region growing was verified to extract a connected vessel tree structure. The initial segmentation was tested with a optimal and automatic selected threshold. The segmentation with the automatic threshold was verified to extract vessel volume without over segmentation, which was a main priority. Compared to the optimal threshold the automatic threshold did extract less vessel volume in each data set. However, the range in volume difference showed a wide range. In some cases the difference was a few hundred voxels. The automatic selection of thresholds may extract a larger volume, if the conservative approach was optimised to the fourteen data set. However, the consequence is over fitting and may cause over segmentation in other data sets.

The initial segmented volume is essential in the bone filter to reduce the removal of vessel volumes. The bone filter was tested with the initial segmented volumes with the optimal and automatic threshold selection, to investigate the difference. In the bone filter adjusted with the volume from the automatic selected threshold, the test showed that in some data sets, the bone filter remove more vessel structures compared to the optimal initial segmented volume. In other data sets the bone filter volume was equal. In the test the bone filter showed varying bone removal quality. However, the bone filter was designed to effectively remove bone structure, which was verified in the test. By investigating the segmented volume profiles e. g. data set 7 and 9, the expense of the bone filter is the removal of big vessels. In these two cases the right external iliac where not segmented.

The filter design was designed with a static intensity threshold and static spatial threshold. Since the size of patients and the image intensities varies among the data, an adaptable bone filter would be appropriate. In addition, the tolerance of vessel volume removal may disqualify the bone filter from other applications where maintenance of all vessel volume is of highest priority. By using the optimal threshold in the initial segmentation none of the bigger vessels was removed with bone filter. However, the optimal threshold was manual selected with the help of a threshold- voxel volume diagrams and visual investigation to assure no over segmentation. The visual inspection is subjective and since a non expert performs the visual evaluation, the results may be subjected to a none optimal threshold selection.

The Extended Segmentation

The test results from the extended segmentation verified that segments with vessel dedicated voxels were extracted. In the test results the extended segmentation showed over segmentation in each data set e. g. by adding a extra volume layer to the initial extracted vessel tree. One reason may relate to the delimitation in the 2D cross section filter, which apply a iteration step on ten instead of one as used in the original method by Graham et al. [2010]. The use of an iteration on ten the intensity cross sections may not produce an optimal elliptic fit.

In the design of the extended segmentation method, the extraction of bone and other high intensity structures was considered and accepted to some extend. The approach was to reject false vessel segments in later processing steps by assuming the merging segmentation would avoid connecting a false vessel segment. The test result showed that the connection scheme in the merging of segmentations was unable to separate vessel dedicated segments from none vessel segment. One

explanation was the simple connection scheme, which relies on region growing and a preset maximum voxels to connect the segments and vessel tree. To discard non vessel segments a more advanced connection schemes is required such as the graph optimization approach in the method by Graham et al. [2010].

Since the original method was developed to extract bronchial tree the intensity required an adaption to the intensities in enhanced vessels, which has a intermediate intensity spectrum in contrary to airways in the lungs. The intermediate intensity approach causes difficulties in the measure of vessel cross section fit. In the original method and the adapted method the cross section is assigned a score based on a mean intensity in the cross section area minus the maximum intensity in the surrounding 4-connected neighbours. This vessel approximation has an intrinsic unbalance when bone structure is located adjacent to the vessel. This unbalance may have caused some over segmentation in the test results.

Merge Segmentations

The vessel tree volume extracted with the merging of segmentation method produced over segmentation in each of the data set. The main reason is assumed to be the lack of vessel fitness in the extended method. Another reason may be the fact that the connection scheme between segments and vessel does not have any predefined criteria on the connected segment or preferred connection direction. The connection scheme purely rely on a intensity similarity to establish the connection. In several data set the initial segmentation was extended in the complete segmentation. By a visually inspection of the vessel tree profiles, the complete segmentation method was able to extract more vessel branches compared to the initial segmentation. However, further tests are needed to estimate the performance of the complete method in terms of accuracy and precision.

13.3 Conclusion

The aim of this work was to develop a segmentation method to extract enhanced vessels in medical images. A main priority was to design a semi automatic method with the minimum amount of manual interaction.

The method is divided in three steps: An initial segmentation to extract a initial vessel tree. An extended segmentation to extract a pool of segments. The last step connect the segments to the initial segmented vessel tree.

The developed segmentation method needs a manual selected seed point as the only manual interaction, thereby successfully fulfilled a semi automatic approach.

The tests shows that the extended method was able to adapt to enhanced vessels in bolus tracked CTA data. However, the segmentation was prone to over segmentation and needs further improvements by optimisation and further development. In conclusion the extended segmentation method was able to adapt a method originally developed for bronchoscopy, to extract enhanced vessels in CTA data. In addition the segmentation as a whole is a semi automatic method that only needs one manual seed point selection.

13.4 Future Work

In this work a three stage segmentation method was presented and tested on CTA data to extract pelvic vessels. The first stage consists of a region growing method with automatic selection of a threshold. The test of the initial segmentation in stage 1 showed a smaller segmented volume compared to a manual selected optimal threshold criteria. In future work the initial segmentation may benefit of using additionally inclusion criteria to maximise the extracted volume without experience over segmentation e.g. by incorporating a derivative domain such as a laplacian or gradient domain [Yang and Holch, 2010; Boskamp et al., 2004].

In the segmentation method a bone removal algorithm was included in the segmentation process to separate vessel dedicated volumes from bone structure. The bone removal proved to be effective in removing large bone volumes. However also vessel dedicated volumes was removed. This suggest further development of a bone filter design with an improved targeting of bone structures e. g. by including an adaption criteria to determine parameter values.

The extended segmentation method in stage 2 was adapted from the work by Graham et al. [2010]; Graham [2008] to segment vessel dedicated segments based on a cross section filter scan and tubular connection between the cross sections. However, in future work additional segmentation stages by Graham et al. [2010] may elaborate the full potential of the method in relation to pelvic artery segmentation. In a recent work by Taeprasartsit [2011] the work was adapted to segmentation of the pulmonary vascular tree and illustrates the generalisability of the method.

Literature

- S. Silbernagl A. Despopulos. *Color Atlas of Physiology*, chapter 8. Cardiovascular System. Number ISBN 3-13-545005-8. Thieme, 5th edition edition, 1998.
- Tobias Boskamp, Daniel Rinck, Florian Link, Bernd Kümmerlen, Georg Stamm, and Peter Mildeberger. New vessel analysis tool for morphometric quantification and visualization of vessels in ct and mr imaging data sets. *Radiographics*, 24(1):287–97, 2004. doi: 10.1148/rg.241035073.
- Encyclopædia Britannica. Prostate cancerer. Encyclopædia Britannica Online, February 2011.
- Cancer.dk, 2011. URL `Cancer.dk`.
- Jesper Carl. Interviews with doctor on aalborg hospital. See Appendix, March 2011.
- Giampiero Ausili Cefaro, Domenico Genovesi, Carlos A. Perez, and Annamaria Vinciguerra. *A Guide for Delineation of Lymph Nodal Clinical Target Volume in Radiation Therapy*, chapter 5. Critical Importance of Target Definition, Including Lymph Nodes, in Image-Guided Radiation Therapy. ISBN: 978354077043. Springer Berlin Heidelberg, 2008.
- K S Clifford Chao and Mary Lin. Lymphangiogram-assisted lymph node target delineation for patients with gynecologic malignancies. *Int J Radiat Oncol Biol Phys*, 54(4):1147–52, Nov 2002.
- Inge Haunstrup Clemmensen, Katrine Hedengran Nedergaard, and Hans Henrik Storm. *Kræft i Danmark en Opslagsbog*. ISBN: 87-7749-330-3. Fagl, 2006.
- Norman Coleman and Edward C. Halperin. *Understanding Cancer: A Patient’s Guide to Diagnosis, Prognosis, and Treatment*, chapter 6. Conventional Treatments: An Overview. Number ISBN: 9780801889547. Johns Hopkins University Press, 2006.
- Ian Cunningham and Philip Judy. *Computed Tomography*. CRC Press, 2011/08/19 1999. ISBN 978-0-8493-8594-0. URL `http://dx.doi.org/10.1201/9781420049510.ch62`.
- Jeffrey Siewerdsen David Jaffray and Mary Gospodarowicz. *Image-Guided Interventions*, chapter 17. Radiation Oncology, pages 501 – 529. Springer Science, 2008.
- Wilfried De Neve. *Image-Guided IMRT*, chapter 1. Rationale of Intensity Modulated Radiation Therapy: A Clinician’s Point of View. Number ISBN: 9783540205111. Springer Berlin Heidelberg, 2006.
- Robert Dinniwell, Philip Chan, Gregory Czarnota, Masoom A Haider, Kartik Jhaveri, Michael Jewett, Anthony Fyles, David Jaffray, and Michael Milosevic. Pelvic lymph node topography for radiotherapy treatment planning from ferumoxtran-10 contrast-enhanced magnetic resonance imaging. *Int J Radiat Oncol Biol Phys*, 74(3):844–51, Jul 2009. doi: 10.1016/j.ijrobp.2008.09.026.

- P. Felkel, R. Wegenkittl, and A. Kanitsar. Vessel tracking in peripheral cta datasets-an overview. In *Computer Graphics, Spring Conference on, 2001.*, pages 232–239, 2001.
- C Florin, N Paragios, and J Williams. Particle filters, a quasi-monte-carlo-solution for segmentation of coronaries. *Medical Image Computing and Computer-Assisted Intervention - Miccai 2005, Pt 1*, 3749:246–253, 2005.
- AF Frangi, WJ Niessen, KL Vincken, and MA Viergever. Multiscale vessel enhancement filtering. *Medical Image Computing and Computer-Assisted Intervention - Miccai'98*, 1496:130–137, 1998.
- Thomas Geeraerts, Vibol Chhor, Gaëlle Cheisson, Laurent Martin, Bertrand Bessoud, Augustin Ozanne, and Jacques Duranteau. Clinical review: initial management of blunt pelvic trauma patients with haemodynamic instability. *Crit Care*, 11(1):204, 2007. doi: 10.1186/cc5157.
- Richard E. Gonzalez, Rafael C.Woods. *Digital Image Processing*. Number ISBN-13: 9780131687288. Pearson Education, inc., 3. ed edition, 2008.
- Michael W. Graham. *Robust Methods for Human Airway -Tree Segmentation and Anatomical-Tree Matching*. Phd thesis, The Pennsylvania State University The Graduate School Department of Electrical Engineering, August 2008.
- Michael W Graham, Jason D Gibbs, Duane C Cornish, and William E Higgins. Robust 3-d airway tree segmentation for image-guided peripheral bronchoscopy. *IEEE Trans Med Imaging*, 29(4): 982–97, Apr 2010. doi: 10.1109/TMI.2009.2035813.
- Calvin Huntzinger, Peter Munro, Scott Johnson, Mika Miettinen, Corey Zankowski, Greg Ahlstrom, Reto Gletting, Reto Filliberti, Wolfgang Kaissl, Martin Kamber, Martin Amstutz, Lionel Bouchet, Dan Klebanov, Hassan Mostafavi, and Richard Stark. Dynamic targeting image-guided radiotherapy. *Med Dosim*, 31(2):113–25, 2006. doi: 10.1016/j.meddos.2005.12.014.
- National Cancer Institute. Cancer staging. Web, February 2011.
- Japan Clinical Oncology Group, Takafumi Toita, Tatsuya Ohno, Yuko Kaneyasu, Takashi Uno, Ryouichi Yoshimura, Takeshi Kodaira, Kazuhisa Furutani, Goro Kasuya, Satoshi Ishikura, Toshiharu Kamura, and Masahiro Hiraoka. A consensus-based guideline defining the clinical target volume for pelvic lymph nodes in external beam radiotherapy for uterine cervical cancer. *Jpn J Clin Oncol*, 40(5):456–63, May 2010. doi: 10.1093/jjco/hyp191.
- Robert Plonsey Karen M. Mudry and Joseph D. Bronzino, editors. *Biomedical Imaging*. Number 978-0-8493-1810-8. CRC Press, 2003.
- M KASS, A WITKIN, and D TERZOPOULOS. Snakes - active contour models. *International Journal of Computer Vision*, 1(4):321–331, 1987.
- C. Kirbas and F. Quek. A review of vessel extraction techniques and algorithms. *Acm Computing Surveys*, 36(2):81–121, 2004.
- Jacobo Kirsch, Eric E. Williamson, and Dominik Fleischmann. *Computed Tomography of the Cardiovascular System*, chapter Computed Tomographic Angiography: Technical Considerations. Number 23 in 9780203089743. Informa Healthcare, first edition edition, 2007.

- Benoit Lengelé and Pierre Scalliet. Anatomical bases for the radiological delineation of lymph node areas. part iii: Pelvis and lower limbs. *Radiother Oncol*, 92(1):22–33, Jul 2009. doi: 10.1016/j.radonc.2008.11.007.
- David Lesage, Elsa D Angelini, Isabelle Bloch, and Gareth Funka-Lea. A review of 3d vessel lumen segmentation techniques: models, features and extraction schemes. *Med Image Anal*, 13(6): 819–45, Dec 2009. doi: 10.1016/j.media.2009.07.011.
- Qingfen Lin. *Enhancement, Extraction, and Visualization of 3D Volume Data*. PhD thesis, Department of Electrical Engineering Linköping University, May 2003.
- L M Lorigo, O D Faugeras, W E Grimson, R Keriven, R Kikinis, A Nabavi, and C F Westin. Curves: curve evolution for vessel segmentation. *Med Image Anal*, 5(3):195–206, Sep 2001.
- Frederic H. Martini, editor. *Fundamentals of Anatomy and Physiology*, chapter 3. The Cellular Level of Organization. Number ISBN: 0-321-31198-1. Pearson Education, inc., 7th edition edition, 2006a.
- Frederic H. Martini, editor. *Fundamentals of Anatomy and Physiology*, chapter 22. The Lymphatic System and Immunity. Number ISBN: 0-321-31198-1. Pearson Education, inc., 7th edition edition, 2006b.
- T McInerney and D Terzopoulos. T-snakes: Topology adaptive snakes. *Medical Image Analysis*, 4(2):73–91, June 2000.
- Jeff M Michalski, Colleen Lawton, Issam El Naqa, Mark Ritter, Elizabeth O’Meara, Michael J Seider, W Robert Lee, Seth A Rosenthal, Thomas Pisansky, Charles Catton, Richard K Valicenti, Anthony L Zietman, Walter R Bosch, Howard Sandler, Mark K Buyyounouski, and Cynthia Ménard. Development of rtog consensus guidelines for the definition of the clinical target volume for postoperative conformal radiation therapy for prostate cancer. *Int J Radiat Oncol Biol Phys*, 76(2):361–8, Feb 2010. doi: 10.1016/j.ijrobp.2009.02.006.
- R Mohan and Thomas Bortfeld. *Image-Guided IMRT*, chapter 2. The Potential and Limitations of IMRT: A Physicist’s Point of View. Number ISBN: 9783540205111. Springer Berlin Heidelberg, 2006.
- SD Olabarriaga, M Breeuwer, and WJ Niessen. Minimum cost path algorithm for coronary artery central axis tracking in ct images. *Medical Image Computing and Computer-Assisted Intervention - Miccai 2003, Pt 2*, 2879:687–694, 2003.
- radiologyinfo. Image-guided radiation therapy. www.radiologyinfo.org, 2011. URL <http://www.radiologyinfo.org/en/info.cfm?pg=IGRT>.
- Mikael Rørth. *Basisbog i Medicin og Kirurgi*, chapter 22. Onkologi, pages 737–748. Munksgaard Danmark, 4 edition, 2007.
- Mikael Rørth and Heine Høi Hansen. *Medicinsk kompendium*, chapter 47: Medicinsk onkologi. Number ISBN: 978-87-17-03933-9. Nyt Nordisk Forlag, 17th edition edition, 2009.
- Marco Schwarz. Clinical implementation: how can imrt become routine? Website Article, February 2009. URL <http://medicalphysicsweb.org/cws/article/opinion/37799>.

- Tobias Souhami, Roberts; Jeffrey. *Cancer and its Management*, chapter 4. Staging Cancer, pages 42–56. John Wiley and Sons, Ltd, 2008a.
- Tobias Souhami, Roberts; Jeffrey. *Cancer and its Management*, chapter 5. Radiotherapy, pages 42–56. John Wiley and Sons, Ltd, 2008b.
- J.S. Suri, Kecheng Liu, L. Reden, and S. Laxminarayan. A review on mr vascular image processing: skeleton versus nonskeleton approaches: part ii. *Information Technology in Biomedicine, IEEE Transactions on*, 6(4):338–350, dec. 2002. ISSN 1089-7771. doi: 10.1109/TITB.2002.804136.
- Higgins W.E. Taeprasartsit, P. Robust method for extracting the pulmonary vascular trees from 3d mdct images. *Progress in Biomedical Optics and Imaging*, 2011.
- A Taylor, A G Rockall, and M E B Powell. An atlas of the pelvic lymph node regions to aid radiotherapy target volume definition. *Clin Oncol (R Coll Radiol)*, 19(7):542–50, Sep 2007. doi: 10.1016/j.clon.2007.05.002.
- Alexandra Taylor, Andrea G Rockall, Rodney H Reznek, and Melanie E B Powell. Mapping pelvic lymph nodes: guidelines for delineation in intensity-modulated radiotherapy. *Int J Radiat Oncol Biol Phys*, 63(5):1604–12, Dec 2005. doi: 10.1016/j.ijrobp.2005.05.062.
- Takashi Uno, Koichi Isobe, Naoyuki Ueno, Hiroki Kobayashi, Yasushi Sanayama, Akira Mitsuhashi, Makio Shozu, and Hisao Ito. Vessel-contouring-based pelvic radiotherapy in patients with uterine cervical cancer. *Jpn J Clin Oncol*, 39(6):376–80, Jun 2009. doi: 10.1093/jjco/hyp029.
- Linda van de Bunt, Uulke A van der Heide, Martijn Ketelaars, Gerard A P de Kort, and Ina M Jürgenliemk-Schulz. Conventional, conformal, and intensity-modulated radiation therapy treatment planning of external beam radiotherapy for cervical cancer: The impact of tumor regression. *Int J Radiat Oncol Biol Phys*, 64(1):189–96, Jan 2006. doi: 10.1016/j.ijrobp.2005.04.025.
- A Vasilevskiy and K Siddiqi. Flux maximizing geometric flows. *Ieee Transactions On Pattern Analysis and Machine Intelligence*, 24(12):1565–1578, December 2002.
- Maria J Vilarino-Varela, Alexandra Taylor, Andrea G Rockall, Rodney H Reznek, and Melanie E B Powell. A verification study of proposed pelvic lymph node localisation guidelines using nanoparticle-enhanced magnetic resonance imaging. *Radiother Oncol*, 89(2):192–6, Nov 2008. doi: 10.1016/j.radonc.2008.07.023.
- WHO. World health organization. <http://www.who.int/mediacentre/factsheets/fs297/en/>, February 2011. URL <http://www.who.int/mediacentre/factsheets/fs297/en/>.
- Wikiradiography. Hounsfield unit. Web: <http://www.wikiradiography.com/page/Hounsfield++unit>, 2011.
- O Wink, WJ Niessen, and MA Viergever. Fast delineation and visualization of vessels in 3-d angiographic images. *Ieee Transactions On Medical Imaging*, 19(4):337–346, April 2000.
- Kenneth H. Wong. *Image-Guided Interventions*, chapter 9. Imaging Modalities, pages 501 – 529. Springer Science, 2008.
- Li Yang and Anders Holch. Delineation of pelvic lymph nodes for image guided radiotherapy in pelvic cancer. Master’s thesis, Aalborg University, July 2010.